

---

# Putting a Face to Forgetting: Continual Learning meets Mechanistic Interpretability

---

Sergi Masip<sup>1</sup> Gido M. van de Ven<sup>2</sup> Javier Ferrando<sup>3</sup> Tinne Tuytelaars<sup>1</sup>

## Abstract

Catastrophic forgetting in continual learning is often measured at the performance or last-layer representation level, overlooking the underlying mechanisms. We introduce a mechanistic framework that offers a geometric interpretation of catastrophic forgetting as the result of transformations to the encoding of individual features. These transformations can lead to forgetting by reducing the allocated capacity of features (worse representation) and disrupting their readout by downstream computations. Analysis of a tractable model formalizes this view, allowing us to identify best- and worst-case scenarios. Through experiments on this model, we empirically test our formal analysis and highlight the detrimental effect of depth. Finally, we demonstrate how our framework can be used in the analysis of practical models through the use of Crosscoders. We present a case study of a Vision Transformer trained on sequential CIFAR-10. Our work provides a new, feature-centric vocabulary for continual learning.

## 1. Introduction

When a neural network trained on one task learns a second, it often catastrophically forgets the first. Current theoretical works largely study this failure from a macroscopic perspective, by analyzing high-level conflicts like task-vector misalignment (Wan et al., 2025), using centered kernel alignment (Kornblith et al., 2019) as a representation similarity measure (Ramasesh et al., 2021), or studying the role of architectural factors like network width (Goldfarb and Hand, 2025; Guha and Lakshman, 2024; Mirzadeh et al., 2022). These studies characterize when interference occurs and what factors correlate with it, but a description of the internal

<sup>1</sup>KU Leuven, Belgium <sup>2</sup>University of Groningen, Netherlands <sup>3</sup>Amazon, Spain. This work is not related to the author's position at Amazon. Correspondence to: Sergi Masip <sergi.masipcabeza@kuleuven.be>, Tinne Tuytelaars <tinne.tuytelaars@kuleuven.be>.

representational transformations associated with forgetting is still lacking.

To fill this gap, our primary contribution is a conceptual framework that offers a granular, mechanistic account of forgetting. We argue that to better understand forgetting, it is valuable to adopt tools that look inside the black box. The field of mechanistic interpretability provides such a lens by aiming to reverse-engineer the algorithms learned by neural networks (Ferrando et al., 2024; Bereska and Gavves, 2024). Its core premise is that knowledge is encoded in a network by hierarchically representing many individual *features*—the fundamental units of representation—which correspond to meaningful concepts or patterns in the data.

Under the mechanistic lens, features are typically assumed to be encoded as *linear directions in activation space* (Olah et al., 2020; Elhage et al., 2022). For each feature, a *feature vector* indicates the direction and strength with which that feature is encoded. Features rarely map cleanly to individual neurons. Neurons are often polysemantic (i.e., encoding multiple features), and networks can represent more features than neurons via *superposition* (Elhage et al., 2022). Superposition translates into a crowded, entangled representation where features compete for *allocated capacity* (Elhage et al., 2022; Scherlis et al., 2022), a geometric measure of how ‘cleanly’ they are represented. A feature with lower allocated capacity has greater overlap with other features and is therefore more difficult to read out.

In this work, we model forgetting as rotations and scaling of feature vectors. As we explain in Section 3.1, rotations can increase *overlap* with other features, while scalings can cause *fading*, both of which reduce a feature’s allocated capacity, compromising its readability. In addition, even if the allocated capacity is not reduced, these transformations can cause *readout misalignment*, where downstream computations no longer extract the information about the feature correctly. Our proposed framework provides a new vocabulary to describe the dynamics underlying forgetting in neural networks.

To illustrate the value of our framework, we use a tractable model to identify best- and worst-case scenarios for feature forgetting during continual learning. We then vali-

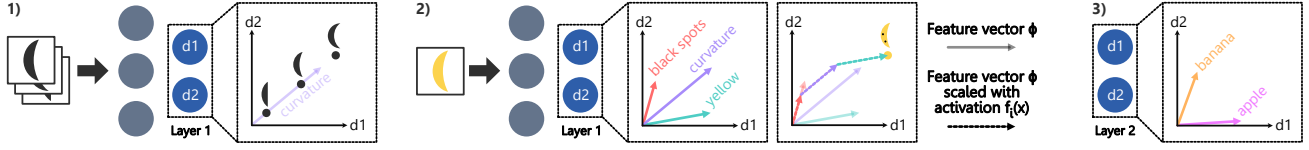


**Figure 1. Linear representation hypothesis.** (1) A feature is a specific concept or pattern in the data (e.g., curvature) that is encoded by a linear direction in a layer’s activation space. The direction and strength with which a feature is represented are captured by a feature vector. (2) These feature vectors form the basis for the layer’s representation: its activation in response to an input  $\mathbf{x}$  is a linear combination of feature vectors  $\phi_i$  weighted by their activations  $f_i(\mathbf{x})$ . (3) Deeper layers encode increasingly abstract features.

date our analytical predictions with an implementation of the tractable model, which empirically supports our analysis. These results provide a fresh explanation for previously observed phenomena related to task similarity (Lee et al., 2021; Hiratani, 2024; Doan et al., 2021) and architectural choices (Guha and Lakshman, 2024; Lu et al., 2024; Mirzadeh et al., 2022). Finally, we apply the framework as a tool to demonstrate its practical implications. Using *crosscoders* (Lindsey et al., 2024), we trace the evolution of features within a Vision Transformer on a standard continual learning vision benchmark, opening new avenues for mechanistic research in continual learning.

Comprehensive discussion of related work in section A.

## 2. Background and terminology

Here, we outline the mechanistic foundations underlying our conceptual framework. First, we explain how the term ‘feature’ is used in this paper (section 2.1), after which we examine how such features occupy representational capacity and how their encodings are read by downstream computations (section 2.2).

### 2.1. Features, the building blocks of representation

A neural network transforms input data into rich numerical representations. With increasing depth, these representations capture increasingly abstract structures and concepts or patterns. In the mechanistic literature, these concepts encoded by the different layers of a neural network are typically called *features*. This means that a feature corresponds to a specific, often highly non-linear, pattern in the input data that is encoded by a particular layer of a neural network.

According to the *linear representation hypothesis* (Mikolov et al., 2013; Elhage et al., 2022; Bereska and Gavves, 2024) (fig. 1), our working assumption, features are encoded as linear directions in a layer’s activation space. Moreover, this hypothesis states that each layer’s activation can be expressed as a linear combination of the activations of all the features that the model has learned to represent in that layer:

$$\mathbf{a}_\ell(\mathbf{x}) = \sum_{i=1}^{n_\ell} f_{\ell,i}(\mathbf{x}) \phi_{\ell,i}. \quad (1)$$

Here,  $\mathbf{a}_\ell(\mathbf{x}) \in \mathbb{R}^{m_\ell}$  is the *representation vector* containing for all  $m_\ell$  neurons in layer  $\ell$  their activation in response to input  $\mathbf{x}$ ,  $n_\ell$  is the number of features encoded by layer  $\ell$ ,  $\phi_{\ell,i} \in \mathbb{R}^{m_\ell}$  is the *feature vector* specifying the direction and strength with which the  $i^{\text{th}}$  feature of layer  $\ell$  is encoded in the representation space of that layer, and  $f_{\ell,i}(\mathbf{x})$  is the *feature activation*, a scalar coefficient measuring how strongly or to what extent the pattern of the  $i^{\text{th}}$  feature of layer  $\ell$  is present in input  $\mathbf{x}$ . When the layer is clear from context, we drop the subscript  $\ell$ .

### 2.2. Representing and reading features

Next, we examine how features are represented and read out. Two aspects matter:

1. **Allocated capacity:** How much of a layer’s representational space is allocated to each feature?
2. **Readout quality:** How effectively do downstream computations extract information about each encoded feature?

Each layer in a neural network has a finite *representational capacity*; it is not possible to linearly represent an unlimited number of features simultaneously without interference. The geometry of the set  $\{\phi_{\ell,i}\}_{i=1}^{n_\ell}$ —in particular the norms (*strength*) and pairwise cosine similarities (*overlap*)—determines the representational capacity allocated to each feature (Elhage et al., 2022).

Features compete for resources, and when they overlap (i.e.,  $\phi_i^\top \phi_j > 0$ ), they share capacity. In practice, features often overlap due to *superposition* (Elhage et al., 2022), a phenomenon that arises when the number of represented features exceeds the available representation dimensions.

The representational capacity given to a feature determines its *inherent readability*—how well it can be recovered from the activation by a linear readout. We can quantify this using the *allocated capacity* (Elhage et al., 2022; Scherlis et al., 2022). This metric captures the “exclusivity” of a feature’s encoding:

$$C_i = \begin{cases} \frac{(\phi_i^\top \phi_i)^2}{\sum_j (\phi_i^\top \phi_j)^2} & \text{if } \|\phi_i\| > 0, \text{ else } 0. \end{cases} \quad (2)$$

When  $\phi_i$  is orthogonal to all other feature vectors  $\phi_j$  in a layer, the feature has exclusive access to its dimension.

When feature vectors overlap, their  $C_i$  decrease, reflecting shared capacity.

Suppose a "yellow" feature  $\phi_i$  is represented in some layer of the network. Downstream computations (subsequent layers) must somehow extract this "yellow" information from the layer's representation. We can model this extraction process using a *readout vector*  $r_i$  (Hänni et al., 2024) that, for any input  $\mathbf{x}$ , attempts to recover the feature's activation  $f_i(\mathbf{x})$  from the layer's representation vector  $\mathbf{a}(\mathbf{x})$ :

$$\mathbf{r}_i^\top \mathbf{a}(\mathbf{x}) \approx f_i(\mathbf{x}). \quad (3)$$

The readout vector  $\mathbf{r}_i$  controls how well the feature is read out by downstream computations, but the quality of this readout is fundamentally limited by the inherent readability of a feature's encoding: a perfect linear readout is only possible when its feature vector is orthogonal to all other feature vectors, i.e.,  $\phi_i^\top \phi_j = 0$  for all  $i \neq j$ , such that its allocated capacity is one ( $C_i = 1$ ). When a feature has allocated capacity lower than one, its readout will always be corrupted by noise from overlapping features.

The distinction between a feature's representation and its readout is key to understanding forgetting in mechanistic terms. It is important to separate a feature's **inherent readability** (its allocated capacity) from its **actual readout quality**, because these two can become misaligned if downstream computations fail to adapt to changes in the feature's representation during continual learning.

### 3. Mechanistic conceptualization of forgetting

We now turn to how the encoding of features changes as the model continues learning. In this section, we introduce a conceptual framework in which forgetting arises from two primitive transformations to individual feature vectors: *rotations* and *scaling*. From this perspective, we show that forgetting arises from capacity degradation due to feature overlap or fading, and from readout misalignment (section 3.1). With a formal tractable model, we show that these effects jointly define the feature dynamics (section 3.2) and enable identifying best- and worst-case scenarios (section 3.3).

#### 3.1. Transformations of feature vectors

**Primitive transformations** During continual learning, neural network parameters get updated, causing feature vectors  $\phi_i$  to undergo transformations that can be decomposed into two primitives: (i) **rotation** ( $\phi_i \rightarrow R^\top \phi_i$ ), which changes the feature vector's direction in representation space, and (ii) **scaling** ( $\phi_i \rightarrow \alpha \phi_i$ ), which alters its magnitude.

**Effects on allocated capacity** A potential consequence of transformations is a change in the network's allocation of capacity to features. *A degradation in a feature's allocated capacity reduces its inherent readability*. The allocated capacity can decrease due to:

- **Overlap:** If  $\phi_i$  rotates towards another feature vector  $\phi_j$ ,  $\phi_i^\top \phi_j$  increases, lowering both  $C_i$  and  $C_j$ .
- **Fading:** Scaling  $\phi_i$  changes the strength of a feature's representation. Scaling affects capacity only when features overlap: reducing its norm (fading) decreases allocated capacity, while increasing its norm (strengthening) boosts its allocated capacity at the expense of others. A feature can thus also lose capacity through strengthening of other overlapping features. In the limit  $\|\phi_i\| \rightarrow 0$ , we say that the feature vanishes, meaning that it is no longer encoded in that layer and can no longer be read out.

**Effects on readout** Even when a feature retains allocated capacity, *transformations can cause feature vectors and readouts to become misaligned*, impairing the quality of the readout. If  $\phi_i$  is scaled down or rotated without updating the readout  $\mathbf{r}_i$ , the next layer reads out a weaker signal or an incorrect feature.

#### 3.2. Dynamics of feature encodings

We now investigate how these transformations and their consequences may arise in a continual learning setup. We assume each task  $T \in \{A, B\}$  is learned sequentially. We use the superscript  $(T)$  to denote that a variable is associated with a task, for example:  $\mathbf{w}^{(T)}$ . We investigate whether and how the similarity between two subsequent tasks influences the forgetting we can expect.

We hypothesize that feature preservation depends on task structure and similarity. Features absent from a new task, or those used consistently across tasks, should remain stable under gradient updates. Conversely, features present but irrelevant to a new task are likely to be transformed to satisfy the new objective. We formalize these dynamics in the following model.

**Model definition** We introduce a simplified *feature-reader model*, which serves as an illustration of how features at a given layer interact with a downstream computation. Similar to the toy autoencoder from Elhage et al. (2022), our model encodes features using feature vectors  $\Phi \in \mathbb{R}^{m \times n} = [\phi_1, \dots, \phi_n]$ , but they are read by a *probe*  $\mathbf{w} \in \mathbb{R}^m$  (a later computation using one or multiple readouts):

$$\hat{y}(\mathbf{x}) = \mathbf{w}^\top \Phi \mathbf{f}(\mathbf{x}). \quad (4)$$

Each task  $T$  assigns a label  $y^T(\mathbf{x})$  to input  $\mathbf{x}$ . In practice, a task would also be defined by a downstream computation.

For tractability, we assume: (i) Feature activations  $f(\mathbf{x})$  are non-negative<sup>1</sup>. (ii) Feature vectors  $\Phi$  are optimized directly, abstracting network parameters. (iii) All relevant features for all tasks are known in advance. Thus, the  $n$  considered features cover all features learned across all tasks. (iv) Each task has a fixed probe  $\mathbf{w}^{(T)}$ ; only  $\Phi$  is updated. This last assumption exaggerates forgetting (section B).

These assumptions isolate the geometry of feature updates. Assumptions (ii) and (iv) permit the closed-form derivation of theorem 3.3 below. All assumptions (i-iv) are needed for theorem 3.4. Relaxing them (e.g., probe adaptation) complicates the analysis, but the hope is that the qualitative conclusions still hold, which we back up with empirical examples in section 4.1.

Note that our model reinterprets the linear model of Saxe et al. (2014) through the mechanistic lens of superposition (Elhage et al., 2022). Their SVD-based analysis cannot represent superposition; our formulation explicitly does.

**Update mechanisms under continual learning** The model is first trained on task  $A$ . Consider a new task  $B$  with a new probe  $\mathbf{w}^{(B)}$ . We train our feature-reader model through gradient descent on task  $B$  using MSE with step size  $\eta$ :

$$\mathcal{L}_B(\mathbf{x}) = \frac{1}{2}(\hat{y}^{(B)}(\mathbf{x}) - y^{(B)}(\mathbf{x}))^2. \quad (5)$$

Before analyzing the gradients and loss, we introduce two quantities that enhance the interpretability of the results.

**Definition 3.1** (Feature contribution  $\beta_i$ ). The *feature contribution* measures how predictive feature  $i$  is for the task:

$$\beta_i^{(T)} := \mathbb{E}_{\mathbf{x}}[y^{(T)}(\mathbf{x})f_i(\mathbf{x})]. \quad (6)$$

Positive values indicate activation for positive labels, and negative values for negative labels. This measure will prove useful to identify important features in practical models (section 5.1).

**Definition 3.2** (Probe sensitivity  $\gamma_i$ ). The *probe sensitivity* measures how strongly the probe relies on feature  $i$ :

$$\gamma_i^{(T)} := (\mathbf{w}^{(T)})^\top \phi_i. \quad (7)$$

A large  $|\gamma_i|$  implies strong reliance on feature  $i$ , with the sign indicating whether it's used for positive or negative predictions. As we will see in section 4 and section 5.1, tracking  $\gamma_i$  over time reveals readout misalignment and fading. If  $\gamma_i$  decreases in later tasks, it means that the probe has lost the ability to read the feature.

<sup>1</sup>This is consistent with sparse autoencoder implementations where activations are ReLU-constrained, and causes some opposing concepts (e.g., dark vs. bright) to split into distinct features.

We now formalize the evolution of feature vectors during training. Using both definitions, we derive how feature vectors evolve under gradient descent on task  $B$ .

**Lemma 3.3** (Expected feature vector update under Task  $B$  training). *Let  $\Sigma_{i,j}^{(T)} := \mathbb{E}_{\mathbf{x} \sim \mathcal{D}_T}[f_i(\mathbf{x})f_j(\mathbf{x})]$ . Under Task  $B$  training, the expected gradient-descent update on feature vector  $\phi_i$  is*

$$\mathbb{E}_{\mathbf{x} \sim \mathcal{D}_B}[\Delta \phi_i] = -\eta \left( \sum_j \gamma_j^{(B)} \Sigma_{ij}^{(B)} - \beta_i^{(B)} \right) \mathbf{w}^{(B)}, \quad (8)$$

*Proof.* See section C.  $\square$

Theorem 3.3 shows that the update for a single feature vector  $\phi_i$  is not only determined by itself but also by correlated feature activations  $f_j$  under a given task. The summation of their alignments with probe  $\mathbf{w}^{(B)}$  must match the feature contribution  $\beta_i^{(B)}$ .

**Best-case scenario for minimal forgetting** Theorem 3.3 reveals two key observations:

- (i) If an old feature  $f_i$  is rarely present in task  $B$  (i.e.,  $\Sigma_{i,j}^{(B)} \approx 0$  for all  $j$  and  $\beta_i^{(B)} \approx 0$ ), then,  $\mathbb{E}_{\mathbf{x} \sim \mathcal{D}_B}[\Delta \phi_i] \approx 0$ . **The feature receives no gradient pressure, constraining forgetting to the active subspace.**
- (ii) The direction of the update is determined by the probe of the new task  $\mathbf{w}^{(B)}$ . Therefore, when task probes are orthogonal ( $\mathbf{w}^{(A)} \perp \mathbf{w}^{(B)}$ ), task  $B$ 's gradients are invisible to task  $A$ , preventing interference.

These observations characterize the best-case for forgetting. However, point (i) no longer holds under regularized optimizers. For instance, **weight decay** introduces fading in inactive or weakly contributing features ( $\beta_i^{(B)} \approx 0$ ), *making some optimizer choices a potential risk factor for forgetting*.

We also provide an analysis of feature dynamics when probes are used across tasks in section D.1, where we find a term that suppresses features predictive for task  $A$ .

### 3.3. Quantifying forgetting in mechanistic terms

Having seen that gradients depend on feature co-activation and probe alignment, we now analyze how much task  $A$  performance degrades when learning task  $B$ . The following result characterizes a scenario in which the feature vectors are replaced by task-optimal solutions, abstracting away optimization path dependence and probe adaptation. While this setting does not model the exact trajectory of gradient descent, it isolates the geometric factors that govern worst-case forgetting: probe alignment, feature co-activation structure, and feature-space regression mismatch.

**Theorem 3.4** (Exact loss-change after learning task  $B$ ). Let  $\mathbf{w}^{(T)} \in \mathbb{R}^m$  be fixed probes for each task, and  $\Phi \in \mathbb{R}^{m \times n}$  be shared and optimized. Denote

$$\mathbf{v}^{(T)} := (\Sigma^{(T)})^\dagger \beta^{(T)}, \quad \alpha := \frac{(\mathbf{w}^{(A)})^T \mathbf{w}^{(B)}}{\|\mathbf{w}^{(B)}\|^2},$$

where  $(\cdot)^\dagger$  is the Moore–Penrose pseudoinverse. Let  $\Phi_{\text{opt}}^{(A)}$  be any minimizer of task  $A$ ’s expected loss and  $\Phi_{\text{opt}}^{(B)} := \frac{\mathbf{w}^{(B)} \mathbf{v}^T}{\|\mathbf{w}^{(B)}\|^2}$  the minimal-Frobenius-norm minimizer for task  $B$ .

Then the exact increase in expected loss on task  $A$  after replacing  $\Phi_{\text{opt}}^{(A)}$  with  $\Phi_{\text{opt}}^{(B)}$  is

$$\begin{aligned} \Delta \mathcal{L}^{(A)} &:= \mathcal{L}^{(A)}(\Phi_{\text{opt}}^{(B)}) - \mathcal{L}^{(A)}(\Phi_{\text{opt}}^{(A)}) \\ &= \frac{1}{2} \|\alpha \mathbf{v}^{(B)} - \mathbf{v}^{(A)}\|_{\Sigma^{(A)}}^2, \end{aligned} \quad (9)$$

where  $\|\cdot\|_{\Sigma^{(A)}}^2$  denotes the quadratic form  $\mathbf{x}^T \Sigma^{(A)} \mathbf{x}$ .

*Proof.* See section E.  $\square$

Theorem 3.4 formally decomposes forgetting  $\Delta \mathcal{L}^{(A)}$  into three core mechanistic quantities: the alignment between task probes ( $\alpha$ ), the statistical structure of features and their coactivations ( $\Sigma$ ), and the minimal-norm feature-space regression coefficient  $\mathbf{v}^{(T)}$  satisfying  $\Sigma^{(T)} \mathbf{v}^{(T)} = \beta^{(T)}$ .

**Worst-case scenario for forgetting** Equation (9) characterizes the worst-case: forgetting is maximized when (1) probes from both tasks are aligned ( $|\alpha|$  large), (2) the task  $A$  and task  $B$  solutions are misaligned ( $|\mathbf{v}^{(A)} - \mathbf{v}^{(B)}|$  large), especially where both tasks require a strong combination of features ( $\|\mathbf{v}\|$  large); and (3) the mismatch lies along ‘loud’ features of task  $A$ , i.e., high-variance directions of  $\Sigma^{(A)}$ .

### 3.4. Conclusions

These results predict the best- and worst-case scenarios for forgetting: disjoint feature sets and orthogonal probes minimize the impact on features and forgetting, while overlapping active subspaces and correlated probes maximize it. This analysis provides formal support for our intuitions on the dynamics of features. Furthermore, our analysis provides a *mechanistic interpretation of the empirically observed U-shaped relationship between task similarity and forgetting*, where intermediately similar tasks (shared but misaligned features) interfere more than either very similar or very dissimilar tasks (disjoint sets of active features), consistent with empirical observations (Ramasesh et al., 2021; Lee et al., 2021; Hiratani, 2024). We next examine whether these theoretical predictions hold empirically.

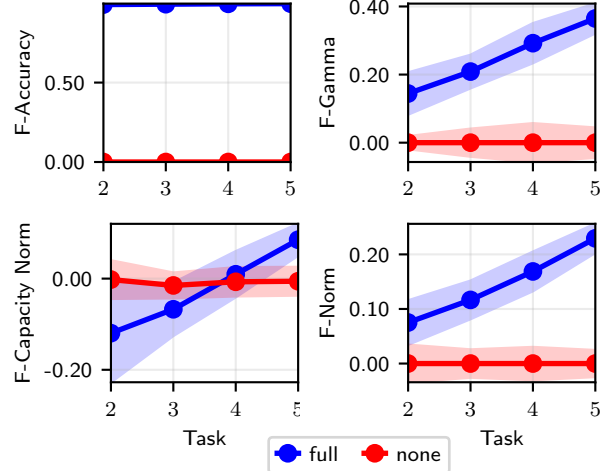


**Figure 2. Effect of shared features on capacity and accuracy forgetting.** Tasks with shared but misaligned features (full) show more forgetting (F-Accuracy) due to misalignment (F-Gamma) and capacity degradation (F-Capacity Norm and F-Norm) than tasks with disjoint sets of features (none).

## 4. Experiments with the feature-reader model

As a first test of our analytical results, we implemented the feature-reader model. The model has a shared one-layer encoder  $\Phi \in \mathbb{R}^{m \times n}$  (with  $n$  features to an  $m$  activation space) and five task-specific linear heads ( $\mathbf{w}^{(T)}$ ). We generated synthetic data for five sequential regression tasks, each defined by a contribution vector  $\beta_t$ . The model was trained with Adam and MSE loss (full experimental details can be found in section F). To analyze the mechanisms of performance drop, we computed the forgetting  $F$  (average degradation for all tasks seen so far) for four key metrics:

- **F-Accuracy:** Derived from raw accuracy  $(1/(1 + \text{MSE}))$ , measuring the loss of task performance.
- **F-Gamma:** Tracks degradation in probe sensitivity ( $\gamma_i$ ).
- **F-Norm:** Tracks reduction in feature vector norms. We use this to explicitly monitor **fading**.
- **F-Capacity Norm:** Tracks  $\hat{C}_i$ , calculated using unit-normalized feature vectors. This metric isolates **feature overlap** from fading, allowing us to disentangle the two sources of capacity degradation.

### 4.1. Results

**Worst- and best-case scenarios** To test the predictions of our formal analysis (section 3.3), we test two conditions: full (predicted worst case), where each task activates all the features ( $\Sigma_{i,j} > 0 \quad \forall i, j$ ) but resamples contributions ( $\beta^{(t)}$ ) to create misaligned task vectors ( $\mathbf{v}^{(t)}$ ) per theorem 3.4, and none (predicted best case), which uses disjoint feature sets ( $\Sigma_{ii}^{(B)} \approx 0$  for task A features) to prevent updates per theorem 3.3. The results in fig. 2 align with theory:

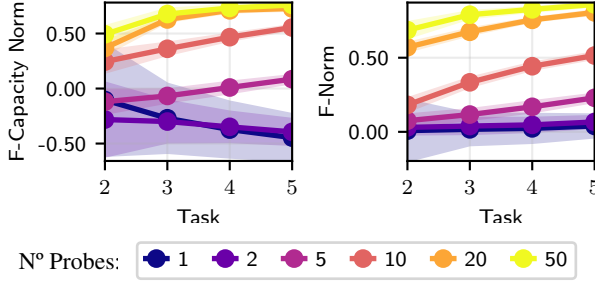


**Figure 3. Impact of the number of probes on allocated capacity.** Increasing the number of probes that read the activation space worsens both overlap (F-Capacity Norm) and fading (F-Norm).

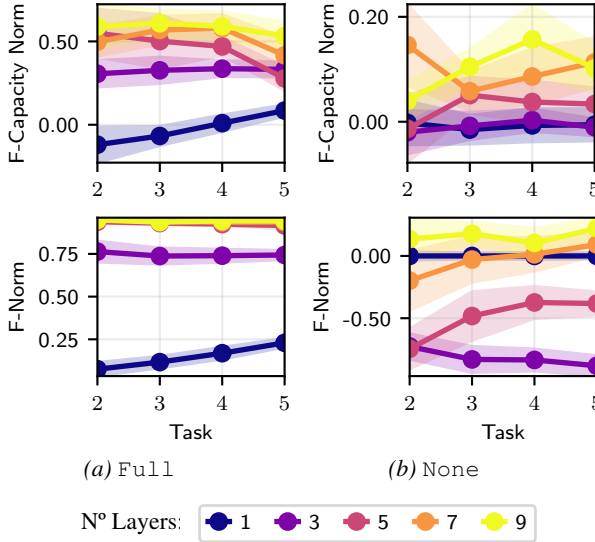


**Figure 4. Effect of depth on allocated capacity.** Depth worsens overlap (F-Capacity Norm) and causes severe fading (F-Norm) in tasks with shared but misaligned features (Full). The effect is milder in features with disjoint sets of active features (None).

none exhibits no accuracy forgetting, whereas full suffers complete accuracy loss. At the feature level, we find capacity degradation, mainly from fading (overlap does not increase until the last task, see the bottom-left plot), and a reduction in  $\gamma$ , indicating increasing readout misalignment.

**Readout saturation worsens capacity forgetting** We next examine how the volume of activation space covered by readouts affects forgetting. Intuitively, increasing the number of probes reduces the chance that any feature remains orthogonal to all probes, thereby limiting its invulnerability to the gradient signal. We focus on the full scenario, since none remains unaffected (theorem 3.3). Figure 3 shows that expanding the number of probes amplifies capacity loss, consistent with the intuition.

**Depth worsens forgetting and fading** In line with prior work (Guha and Lakshman, 2024; Lu et al., 2024), we found that network depth can strongly influence forgetting. To as-

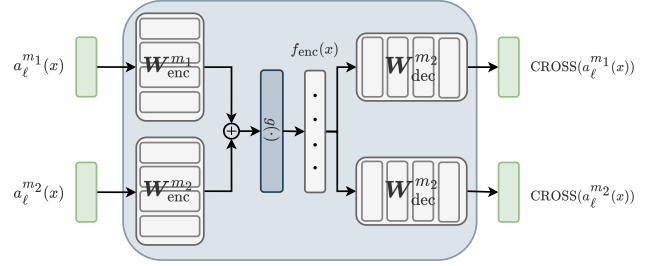


**Figure 5. Crosscoder diagram:** Representations  $a_\ell^{m1}(x)$  from multiple models are mapped to a single shared latent space  $f_{enc}(x)$ , which is then used by model-specific decoders to reconstruct the original activations.

sess this effect and scale up to realistic models, we extended the encoder of the model, which parameterized the feature vectors, with additional layers. Note that we did not add nonlinearities, thus keeping the model’s linear expressiveness, which allowed us to isolate the effects of depth cleanly.

For each feature  $i$ , we studied its direction in activation space via  $\mathbb{1}_i^\top \Phi$ , where  $\mathbb{1}_i$  is a zero matrix with a 1 in the  $i$ -th diagonal position. As shown in fig. 4, depth impacts full and none differently. In full, deeper encoders markedly reduce feature norms. In contrast, none displays roughly a constant normalized capacity and negative norm forgetting, i.e., feature norms increase across tasks. However, forgetting becomes positive beyond seven layers.

One possible explanation is that, in deep linear networks, scaling feature magnitudes provides a simpler optimization pathway than coordinated rotations across layers. We leave a formal analysis of this hypothesis to future work.

## 5. Scaling up with crosscoders

Our feature-reader model provided key mechanistic insights, such as the detrimental effect of depth, using a simplified setting where the features were known. To apply our framework to deep networks, we must first identify their features, which are often unknown and entangled in superposition. Below, we discuss tools that allow us to approximate and track these features in practical models.

**Sparse autoencoders (SAEs)** (Bricken et al., 2023) separate and identify features in superposition by mapping layer activations  $a_\ell(\mathbf{x}) \in \mathbb{R}^{d_{\text{model}}}$  to a higher-dimensional sparse space ( $d_{\text{cross}} > d_{\text{model}}$ ):

$$f_{\text{enc}}(\mathbf{x}) = g(\mathbf{W}_{\text{enc}} a_\ell(\mathbf{x}) + \mathbf{b}_{\text{enc}}) \quad (10)$$

$$\text{SAE}(\mathbf{x}) = \mathbf{W}_{\text{dec}} f_{\text{enc}}(\mathbf{x}) + \mathbf{b}_{\text{dec}} \quad (11)$$

Each latent unit  $f_{\text{enc},i}(\mathbf{x})$  corresponds to a feature activation, and each decoder column  $\mathbf{W}_{\text{dec},i}$  represents its contribution to the reconstructed activation.

**Crosscoders** (Lindsey et al., 2024) generalize SAEs to com-



Figure 6. Activation maps for the most important feature from task 1. Shown are the images that most strongly activated this feature at each task. The bottom row overlays these images with their corresponding activation maps. The feature appears to be activated by the background parts of the image.

pare models or layers by learning a *shared latent feature space* across representations  $\mathbf{a}_\ell^{m_t}(\mathbf{x})$  from multiple models  $m_t \in \mathcal{M}$ :

$$\mathbf{f}_{\text{enc}}(\mathbf{x}) = g\left(\sum_{m_t \in \mathcal{M}} \mathbf{W}_{\text{enc}}^{m_t} \mathbf{a}_\ell^{m_t}(\mathbf{x}) + \mathbf{b}_{\text{enc}}\right). \quad (12)$$

Model-specific decoders  $\mathbf{W}_{\text{dec}}^{m_t}$  reconstruct each model’s activations through

$$\text{CROSS}^{m_t}(\mathbf{a}_\ell^{m_t}(\mathbf{x})) = \mathbf{W}_{\text{dec}}^{m_t} \mathbf{f}_{\text{enc}}(\mathbf{x}) + \mathbf{b}_{\text{dec}}. \quad (13)$$

A schematic overview is shown in Figure 5, and a detailed introduction is provided in section G.

This formulation embeds our conceptual framework (Section 3) in practical models. Note, however, that crosscoder features should not be interpreted as ground-truth. We treat the global feature basis defined by the encoders as an approximation of the true  $\mathbf{f}(\mathbf{x})$ , and each decoder column  $\mathbf{W}_{\text{dec},i}^{m_t}$  as a feature vector  $\phi_i^{(t)}$ . This enables approximate tracking of features across training stages.

### 5.1. A practical case study with a ViT

To demonstrate how real models can be studied under our framework, we apply crosscoders to a practical case study: a Vision Transformer (ViT) sequentially trained on CIFAR-10. While our tractable model analyzed the direct gradient dynamics of known feature vectors  $\Phi$ , this ViT analysis will track their analogs—the crosscoder’s decoder vectors ( $\mathbf{W}_{\text{dec},i}^{m_t}$ )—to study the same geometric transformations.

**Setup** We train a ViT (Dosovitskiy et al., 2021) on Split CIFAR-10 (Krizhevsky, 2009) (five tasks, two classes per task), under a task-incremental learning setup (Van de Ven et al., 2022) (one head per task) across four seeds. We train a separate crosscoder for each seed. For each task  $t$ , we analyze its model  $m_t$  by selecting the top five features ranked by importance,  $I_i^{(t)} = \beta_i^{(t)} \cdot \gamma_i^{(t)}$ . This product captures features that are both highly predictive for the task (high  $\beta_i^{(t)}$ ) and strongly relied upon by the model’s readout (high  $\gamma_i^{(t)}$ ). Full setup details are in section H.

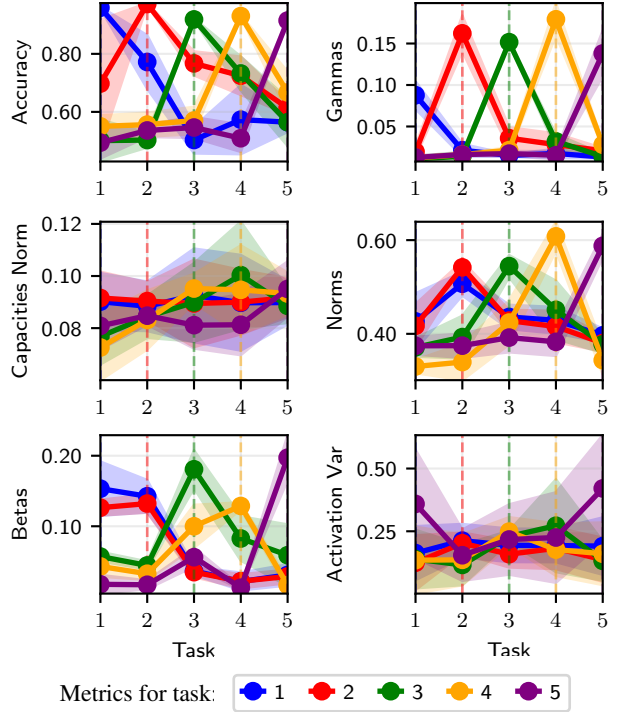


Figure 7. Metrics evolution across tasks for the penultimate layer. Shown is the average value for each metric over the top-5 most important features of each task.

**Forgetting driven by fading and misalignment** Figure 7 shows that each task’s accuracy drops as new tasks are learned despite a largely stable normalized capacity. This indicates that severe overlap between features is not the main issue. Instead, forgetting correlates more with *misalignment and fading* in this setting. Note that all features remain active across tasks (bottom-right plot), but their contribution (bottom-left plot) changes substantially. This is consistent with the *worst-case scenario* described by our theory: when feature directions persist but their scaling and readout drift, the system retains structure yet loses predictive power. The observed dominance of fading over rotation aligns with trends seen in the feature-reader model under increasing depth (section 4.1). A notable exception occurs after the second task, where norms increase, likely due to the strong similarity and shared features between the first and second tasks, as indicated by their closely aligned  $\beta$  values.

**Testing misalignment as the culprit** We performed an intervention to isolate misalignment, crafting a classifier head by linearly combining the evolved decoder vectors  $\mathbf{W}_{\text{dec},i}^{m_t}$  weighted by their initial importance  $I_i^{(t)}$ . This restores the original readout alignment. We compare against the original classifier and a random combination of decoder vectors.

As shown in fig. 8, accuracy was recovered only for task 1

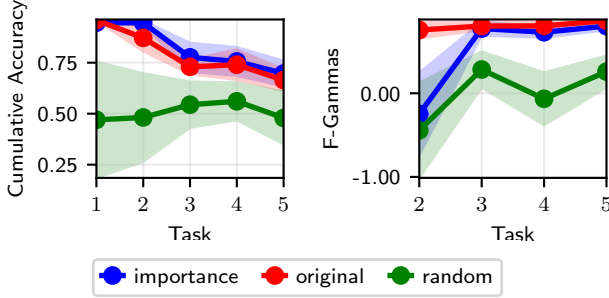


Figure 8. Comparison of intervened classifier and baselines. The intervened classifier mitigates misalignment, indicating that fading dominates forgetting.

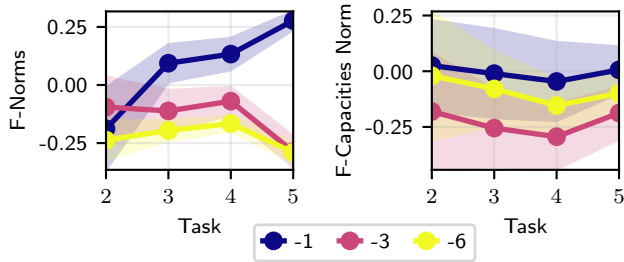


Figure 9. Capacity metrics for different layers of the ViT. While the last layer’s capacity degrades, earlier layers grow theirs.

(which shares features with task 2), and only marginally for the others, indicating that fading is the dominant factor in performance decay. The high forgetting observed in  $\gamma$  is not evidence of rotational misalignment, but is a direct result of this fading (norm reduction). Figure 7 confirms this: while the norms of key features increase during training on the task, they subsequently decrease as the model reallocates capacity to newer tasks.

**Earlier layers grow their capacity** A natural next question is whether this pattern holds across layers. Prior work (Yosinski et al., 2014; Ramasesh et al., 2021) reports that earlier layers remain stable while forgetting mainly arises in the final layers. Surprisingly, fig. 9 shows that earlier layers *gain* allocated capacity over time. As new tasks are learned, feature norms increase in these layers.

## 6. Discussion and limitations

We have bridged continual learning and mechanistic interpretability, which has resulted in a conceptual framework that provides a granular vocabulary for forgetting. We have studied a toy model that we refer to as the feature-reader model, which functions as a proxy for analyzing the mechanisms of feature forgetting in practical neural networks. Similar toy models have proven valuable in prior work (El-hage et al., 2022; Hänni et al., 2024) in unveiling phenomena such as superposition. In this paper, we used the framework

to gain a better mechanistic understanding of catastrophic forgetting. In future work, the framework could be used to gain such understanding about other continual learning phenomena, such as the stability gap (De Lange et al., 2023).

As is common in the mechanistic literature, our work relies on the linear representation hypothesis. Although recent work shows that some features are multidimensional, such as the days of the week (Engels et al., 2024), substantial evidence supports the hypothesis across diverse contexts (Arora et al., 2018; O’Mahony et al., 2023; Bricken et al., 2023). We also assume that the hypothesis remains valid during continual learning. Yet when a feature fades, it could also be questioned whether the feature is still linear.

To demonstrate how our framework can be applied to practical models, we studied feature dynamics in a ViT continually trained on Split CIFAR-10. While the results revealed fading predominance and layer-wise capacity dynamics—insights that would be obscured by high-level metrics—they should be considered preliminary given the limited scale of this demonstration. Also, we caution that SAEs are empirical tools with limitations. They are not foolproof (Song et al., 2025) and can be difficult to tune, as feature decompositions are approximate and sensitive to modeling choices.

Despite these limitations, our framework has its own merits. While diagnostic tools such as linear probing or centered kernel alignment (CKA) are valuable for detecting representational drift, they often do not distinguish between the specific manifestations identified in this work: overlap, fading, and readout misalignment. For example, a drop in CKA signals a change but does not specify if the features have rotated (requiring orthogonalization) or faded (requiring norm preservation). Our framework addresses this gap, offering practitioners a semantic lens to diagnose future methods and, e.g., determine what knowledge to retain or forget.

## 7. Conclusions

We have introduced a new, feature-centric framework that bridges continual learning and mechanistic interpretability. We showed how forgetting can be interpreted as the result of geometric transformations that reduce the allocated capacity of features or cause readout misalignment. We characterized the best and worst scenarios for forgetting and formalized this in a tractable feature-reader model. Empirical validation of this model also revealed the detrimental effect of depth on allocated capacity. Finally, we have demonstrated how this analysis can be scaled up to practical models through the use of crosscoders. In a controlled ViT case study, feature fading and readout misalignment emerged as dominant correlates of forgetting, particularly at the last layer. This work provides a new vocabulary for diagnosing CL failures and deepening the understanding of forgetting.

## Acknowledgements

We want to thank Pau Rodríguez and Timm Hess for their valuable feedback and advice. We also appreciate the rich discussions with Jonathan Swinnen, Milan van Maldegem, Zehao Wang, Minye Wu, and Matthew Blaschko.

This paper has received funding from the Flemish Government under the Methusalem Funding Scheme (grant agreement n° METH/24/009).

## References

Sanjeev Arora, Yuanzhi Li, Yingyu Liang, Tengyu Ma, and Andrej Risteski. Linear algebraic structure of word senses, with applications to polysemy. *Transactions of the Association for Computational Linguistics*, 6:483–495, 2018.

Mehdi Abbana Bennani, Thang Doan, and Masashi Sugiyama. Generalisation guarantees for continual learning with orthogonal gradient descent. *arXiv preprint arXiv:2006.11942*, 2020.

Leonard Bereska and Stratis Gavves. Mechanistic interpretability for AI safety - a review. *Transactions on Machine Learning Research*, 2024. Survey Certification, Expert Certification.

Trenton Bricken, Adly Templeton, Joshua Batson, Brian Chen, Adam Jermyn, Tom Conerly, Nick Turner, Cem Anil, Carson Denison, Amanda Askell, Robert Lasenby, Yifan Wu, Shauna Kravec, Nicholas Schiefer, Tim Maxwell, Nicholas Joseph, Zac Hatfield-Dodds, Alex Tamkin, Karina Nguyen, Brayden McLean, Josiah E Burke, Tristan Hume, Shan Carter, Tom Henighan, and Christopher Olah. Towards monosemanticity: Decomposing language models with dictionary learning. *Transformer Circuits Thread*, 2023. <https://transformer-circuits.pub/2023/monosemantic-features/index.html>.

Matthias De Lange, Gido M van de Ven, and Tinne Tuytelaars. Continual evaluation for lifelong learning: Identifying the stability gap. In *The Eleventh International Conference on Learning Representations*, 2023.

Meng Ding, Kaiyi Ji, Di Wang, and Jinhui Xu. Understanding forgetting in continual learning with linear regression. In *Proceedings of the 41st International Conference on Machine Learning*, pages 10978–11001, 2024.

Thang Doan, Mehdi Abbana Bennani, Bogdan Mazoure, Guillaume Rabusseau, and Pierre Alquier. A theoretical analysis of catastrophic forgetting through the ntk overlap matrix. In *International Conference on Artificial Intelligence and Statistics*, pages 1072–1080. PMLR, 2021.

Alexey Dosovitskiy, Lucas Beyer, Alexander Kolesnikov, Dirk Weissenborn, Xiaohua Zhai, Thomas Unterthiner, Mostafa Dehghani, Matthias Minderer, Georg Heigold, Sylvain Gelly, Jakob Uszkoreit, and Neil Houlsby. An image is worth 16x16 words: Transformers for image recognition at scale. In *International Conference on Learning Representations*, 2021.

Nelson Elhage, Tristan Hume, Catherine Olsson, Nicholas Schiefer, Tom Henighan, Shauna Kravec, Zac Hatfield-Dodds, Robert Lasenby, Dawn Drain, Carol Chen, et al. Toy models of superposition. *arXiv preprint arXiv:2209.10652*, 2022.

Joshua Engels, Eric J Michaud, Isaac Liao, Wes Gurnee, and Max Tegmark. Not all language model features are linear. *arXiv preprint arXiv:2405.14860*, 2024.

Itay Evron, Edward Moroshko, Rachel Ward, Nathan Srebro, and Daniel Soudry. How catastrophic can catastrophic forgetting be in linear regression? In *Conference on Learning Theory*, pages 4028–4079. PMLR, 2022.

Itay Evron, Edward Moroshko, Gon Buzaglo, Maroun Khriesh, Badea Marjeh, Nathan Srebro, and Daniel Soudry. Continual learning in linear classification on separable data. In *International Conference on Machine Learning*, pages 9440–9484. PMLR, 2023.

Javier Ferrando, Gabriele Sarti, Arianna Bisazza, and Marta R. Costa-jussà. A primer on the inner workings of transformer-based language models, 2024.

Leo Gao, Tom Dupre la Tour, Henk Tillman, Gabriel Goh, Rajan Troll, Alec Radford, Ilya Sutskever, Jan Leike, and Jeffrey Wu. Scaling and evaluating sparse autoencoders. In *The Thirteenth International Conference on Learning Representations*, 2025.

Daniel Goldfarb and Paul Hand. Analysis of catastrophic forgetting for random orthogonal transformation tasks in the overparameterized regime. In *Proceedings of The 26th International Conference on Artificial Intelligence and Statistics*, pages 2975–2993. PMLR, 2023.

Daniel Goldfarb and Paul Hand. Analysis of overparameterization in continual learning under a linear model. *arXiv*, 2502.10442, 2025.

Etash Kumar Guha and Vihan Lakshman. On the diminishing returns of width for continual learning. In *International Conference on Machine Learning*, pages 16706–16730. PMLR, 2024.

Wes Gurnee, Neel Nanda, Matthew Pauly, Katherine Harvey, Dmitrii Troitskii, and Dimitris Bertsimas. Finding neurons in a haystack: Case studies with sparse probing. *Transactions on Machine Learning Research*, 2023.

Kaarel Hänni, Jake Mendel, Dmitry Vaintrob, and Lawrence Chan. Mathematical models of computation in superposition. *arXiv preprint arXiv:2408.05451*, 2024.

Naoki Hiratani. Disentangling and mitigating the impact of task similarity for continual learning. *arXiv preprint arXiv:2405.20236*, 2024.

Chenhui Hu, Pengfei Cao, Yubo Chen, Kang Liu, and Jun Zhao. Knowledge in superposition: Unveiling the failures of lifelong knowledge editing for large language models. *arXiv preprint arXiv:2408.07413*, 2024.

Robert Huben, Hoagy Cunningham, Logan Riggs Smith, Aidan Ewart, and Lee Sharkey. Sparse autoencoders find highly interpretable features in language models. In *The Twelfth International Conference on Learning Representations*, 2024.

Sagar Imambi, Kolla Bhanu Prakash, and GR Kanagachidambaram. Pytorch. In *Programming with TensorFlow: solution for edge computing applications*, pages 87–104. Springer, 2021.

Olaf Yunus Laitinen Imanov. Mechanistic analysis of catastrophic forgetting in large language models during continual fine-tuning, 2026.

Hyunji Jung, Hanseul Cho, and Chulhee Yun. Convergence and implicit bias of gradient descent on continual linear classification. *arXiv preprint arXiv:2504.12712*, 2025.

Jeremias Knoblauch, Hisham Husain, and Tom Diethe. Optimal continual learning has perfect memory and is np-hard. In *International Conference on Machine Learning*, pages 5327–5337. PMLR, 2020.

Simon Kornblith, Mohammad Norouzi, Honglak Lee, and Geoffrey Hinton. Similarity of neural network representations revisited. In *International conference on machine learning*, pages 3519–3529. PMLR, 2019.

Alex Krizhevsky. Learning multiple layers of features from tiny images. Technical report, University of Toronto, 2009.

Sebastian Lee, Sebastian Goldt, and Andrew Saxe. Continual learning in the teacher-student setup: Impact of task similarity. In *International Conference on Machine Learning*, pages 6109–6119. PMLR, 2021.

Jack Lindsey, Adly Templeton, Marcus Jonathan, Thomas Conerly, Joshua Batson, , and Christopher Olah. Sparse crosscoders for cross-layer features and model diffing. *Transformer Circuits Thread*, 2024.

Aojun Lu, Tao Feng, Hangjie Yuan, Xiaotian Song, and Yanan Sun. Revisiting neural networks for continual learning: An architectural perspective. In *IJCAI*, 2024.

Michael McCloskey and Neal J Cohen. Catastrophic interference in connectionist networks: The sequential learning problem. In *Psychology of Learning and Motivation*, pages 109–165. Elsevier, 1989.

Tomáš Mikolov, Wen-tau Yih, and Geoffrey Zweig. Linguistic regularities in continuous space word representations. In *Proceedings of the 2013 conference of the north american chapter of the association for computational linguistics: Human language technologies*, pages 746–751, 2013.

Seyed Iman Mirzadeh, Arslan Chaudhry, Dong Yin, Huiyi Hu, Razvan Pascanu, Dilan Gorur, and Mehrdad Farajtabar. Wide neural networks forget less catastrophically. In *International conference on machine learning*, pages 15699–15717. PMLR, 2022.

Jesse Mu and Jacob Andreas. Compositional explanations of neurons. *Advances in Neural Information Processing Systems*, 33:17153–17163, 2020.

Chris Olah, Nick Cammarata, Ludwig Schubert, Gabriel Goh, Michael Petrov, and Shan Carter. Zoom in: An introduction to circuits. *Distill*, 2020. <https://distill.pub/2020/circuits/zoom-in>.

Laura O’Mahony, Vincent Andrearzyk, Henning Müller, and Mara Graziani. Disentangling neuron representations with concept vectors. In *Proceedings of the IEEE/CVF Conference on Computer Vision and Pattern Recognition*, pages 3770–3775, 2023.

Vinay Venkatesh Ramasesh, Ethan Dyer, and Maithra Raghu. Anatomy of catastrophic forgetting: Hidden representations and task semantics. In *International Conference on Learning Representations*, 2021.

Roger Ratcliff. Connectionist models of recognition memory: constraints imposed by learning and forgetting functions. *Psychological Review*, 97:285–308, 1990.

A Saxe, J McClelland, and S Ganguli. Exact solutions to the nonlinear dynamics of learning in deep linear neural networks. In *Proceedings of the International Conference on Learning Representations 2014*. International Conference on Learning Representations 2014, 2014.

Adam Scherlis, Kshitij Sachan, Adam S Jermyn, Joe Benton, and Buck Shlegeris. Polysemanticity and capacity in neural networks. *arXiv preprint arXiv:2210.01892*, 2022.

Xiangchen Song, Aashiq Muhammed, Yujia Zheng, Lingjing Kong, Zeyu Tang, Mona T. Diab, Virginia Smith, and Kun Zhang. Position: Mechanistic interpretability should prioritize feature consistency in saes, 2025.

Adly Templeton, Tom Conerly, Jonathan Marcus, Jack Lindsey, Trenton Bricken, Brian Chen, Adam Pearce, Craig Citro, Emmanuel Ameisen, Andy Jones, Hoagy Cunningham, Nicholas L Turner, Callum McDougall, Monte MacDiarmid, C. Daniel Freeman, Theodore R. Sumers, Edward Rees, Joshua Batson, Adam Jermyn, Shan Carter, Chris Olah, and Tom Henighan. Scaling monosemanticity: Extracting interpretable features from claude 3 sonnet. *Transformer Circuits Thread*, 2024.

Gido M Van de Ven, Tinne Tuytelaars, and Andreas S Tolias. Three types of incremental learning. *Nature Machine Intelligence*, 4 (12):1185–1197, 2022.

Hongyi Wan, Shiyuan Ren, Wei Huang, Miao Zhang, Xiang Deng, Yixin Bao, and Liqiang Nie. Understanding the forgetting of (replay-based) continual learning via feature learning: Angle matters. In *Forty-second International Conference on Machine Learning*, 2025.

Jason Yosinski, Jeff Clune, Yoshua Bengio, and Hod Lipson. How transferable are features in deep neural networks? *Advances in neural information processing systems*, 27, 2014.

Fei Zhu, Yujing Liu, Wenzhuo Liu, and Zhaoxiang Zhang. Global convergence of continual learning on non-iid data. *arXiv preprint arXiv:2503.18511*, 2025.

## A. Comprehensive related work

### A.1. Theoretical and conceptual understanding of catastrophic forgetting

Catastrophic forgetting, first identified decades ago (McCloskey and Cohen, 1989; Ratcliff, 1990), remains a central challenge in continual learning. While many methods have been proposed to mitigate it, a complete theoretical account is still developing. Early intuitions framed forgetting with high-level concepts like "weight drift" or "interference", but these lack the precision needed for a deep, mechanistic understanding.

Recent theoretical work has sought to add rigor from several angles:

**Formalisms, bounds, and convergence** Earlier works formalized the continual learning problem and its scenarios (Van de Ven et al., 2022) and showed that continual learning is NP-hard by relating it to a set intersection decision problem (Knoblauch et al., 2020). Recently, a significant body of work uses simplified settings, particularly linear models, to achieve analytical tractability. These studies have provided valuable insights, including deriving performance bounds (Evron et al., 2022; 2023; Ding et al., 2024), proving convergence to joint solutions in cyclic learning (Jung et al., 2025), and proving global convergence in continual settings (Zhu et al., 2025). In line with these works, we also employ a tractable linear model. However, where much of this work focuses on proving convergence or bounding final performance, our goal is to reveal the internal geometric dynamics of how representations are transformed and evolve during continual learning.

**Task similarity and gradient alignment** Another prominent line of research investigates how the relationship between tasks influences forgetting. Forgetting is often framed as a consequence of misaligned task gradients or competition for representational subspaces. Studies have shown a U-shaped relationship where intermediate task similarity can cause the most interference (Ramasesh et al., 2021; Lee et al., 2021; Hiratani, 2024). Other work operating in the neural tangent kernel regime has linked forgetting to the parameter-space alignment of task updates (Bennani et al., 2020; Doan et al., 2021). In a recent publication, Wan et al. (2025) claimed that the cosine similarity between task "signal vectors" determines the degree of forgetting, with anti-aligned tasks being the most detrimental.

These works successfully predict that certain task configurations cause forgetting, but they do not explain the representational mechanisms by which this forgetting occurs. Task-level metrics (vector alignment, subspace overlap) describe the conditions for interference but remain agnostic to the specific geometric transformations and capacity reallocation that degrade individual features. Our framework complements these predictive models by providing a mechanistic account of the internal dynamics they summarize. We decompose these high-level task conflicts into interpretable geometric transformations of the underlying feature vectors, directly linking them to changes in capacity and readout.

**Architectural factors** The role of model architecture is also a key area of study. Overparameterization, particularly width, has been shown to mitigate forgetting, often by enabling a "lazy" training regime where parameters stay close to their initialization (Goldfarb and Hand, 2023; 2025; Mirzadeh et al., 2022; Guha and Lakshman, 2024; Lu et al., 2024). Our mechanistic framework could complement these findings by offering a potential explanation for how more capacity (i.e., more dimensions) can reduce the destructive feature overlap that causes forgetting, particularly by allowing more room for features to stay orthogonal to any readout.

**Linear dynamics analysis** Theorem 3.3 reinterprets the linear network dynamics of Saxe et al. (2014) through the mechanistic lens of superposition (Elhage et al., 2022). Saxe et al. (2014) decomposed the input-output covariance matrix ( $\Sigma^{31}$  in their work) via SVD and described the dynamics of "connectivity modes"; The number of modes is limited to the rank of  $\Sigma^{31}$ . Superposition, however, creates a "congested" representation that an SVD-based analysis cannot fully capture. Our framework explicitly models superposition.

### A.2. Mechanistic interpretability

To build our feature-level account of forgetting, we draw on tools and concepts from the field of mechanistic interpretability, which aims to reverse-engineer the internal computations of neural networks.

**Features, polysemy, and superposition** A central finding in this field is that knowledge is not typically stored in individual neurons. Instead, neurons are often polysemantic, participating in the representation of multiple concepts (Mu and Andreas, 2020). The fundamental unit of representation is therefore considered the feature, which is best understood as

a direction in a layer’s activation space (Olah et al., 2020; Elhage et al., 2022). Certain architectural choices or conditions, such as specific non-linearities allow a model to learn more features than it has neurons (or dimensions). This phenomenon is known as superposition. Superposition may be possible following the Johnson–Lindenstrauss lemma, which states that  $\exp(m)$  vectors can be placed almost-orthogonally in an  $m$ -dimensional space. Recent evidence points to the existence of superposition in deep neural networks, including large language models (Gurnee et al., 2023; Templeton et al., 2024).

**Capacity and interference** Superposition has a direct cost: features must compete for finite representational resources. The geometry of the feature vectors—their norms and pairwise inner products—determines the allocated capacity for each feature, a measure of how cleanly it can be distinguished from others (Elhage et al., 2022; Scherlis et al., 2022). This concept is crucial for our work. Pioneering research has suggested that superposition is a primary cause of interference in related problems like lifelong model editing (Hu et al., 2024), and concurrent work has empirically studied forgetting in LLMs using mechanistic insights (Imanov, 2026).

Our work explicitly links the mechanistic concepts of superposition and allocated capacity to catastrophic forgetting in continual learning. By synthesizing these two fields, our work provides a new lens through which to understand the geometric and representational roots of catastrophic forgetting. We move beyond describing *that* forgetting happens and aim to explain precisely *how* it happens at the level of the model’s fundamental building blocks: its features.

## B. Effect of probe-feature co-adaptation

**Proposition B.1** (Gradient load sharing between probe and features). *Let the feature–reader model be defined as*

$$\hat{y}(x) = w_B^\top \Phi f(x),$$

*with loss*

$$L_B = \frac{1}{2} \mathbb{E}_{x \sim D_B} [(\hat{y}(x) - y_B(x))^2].$$

*Denote by  $\Phi = [\phi_1, \dots, \phi_n] \in \mathbb{R}^{m \times n}$  the feature matrix and by  $w_B \in \mathbb{R}^m$  the probe for task B. Let*

$$\Sigma_{ij}^{(B)} = \mathbb{E}[f_i(x)f_j(x)], \quad \beta_i^{(B)} = \mathbb{E}[y_B(x)f_i(x)].$$

*Then, under simultaneous gradient descent updates*

$$\Delta w_B = -\eta_w \nabla_{w_B} L_B, \quad \Delta \phi_i = -\eta_\phi \nabla_{\phi_i} L_B,$$

*the expected parameter updates satisfy*

$$\mathbb{E}_{x \sim D_B} [\Delta w_B] = -\eta_w (\Phi \Sigma^{(B)} \Phi^\top w_B - \Phi \beta^{(B)}),$$

$$\mathbb{E}_{x \sim D_B} [\Delta \phi_i] = -\eta_\phi ((w_B^\top \Phi \Sigma^{(B)})_i - (w_B^\top \beta^{(B)})_i) w_B.$$

*Consequently, the infinitesimal reduction in expected loss can be decomposed as*

$$\mathbb{E}[\Delta L_B] = -\eta_w \|\nabla_{w_B} L_B\|^2 - \eta_\phi \sum_i \|\nabla_{\phi_i} L_B\|^2,$$

*which quantifies the gradient load sharing between probe and feature parameters. The relative share handled by each group is*

$$\rho_w = \frac{\|\nabla_{w_B} L_B\|^2}{\|\nabla_{w_B} L_B\|^2 + \sum_i \|\nabla_{\phi_i} L_B\|^2}, \quad \rho_\phi = 1 - \rho_w.$$

*Proof.* Expanding the loss:

$$L_B = \frac{1}{2} \mathbb{E}[(w_B^\top \Phi f - y_B)^2].$$

Taking the gradient with respect to  $w_B$ :

$$\nabla_{w_B} L_B = \mathbb{E}[(w_B^\top \Phi f - y_B) \Phi f] = (\Phi \Sigma^{(B)} \Phi^\top) w_B - \Phi \beta^{(B)}.$$

This yields the expected probe update

$$\mathbb{E}[\Delta w_B] = -\eta_w [(\Phi \Sigma^{(B)} \Phi^\top) w_B - \Phi \beta^{(B)}].$$

Next, for a single feature vector  $\phi_i$ :

$$\nabla_{\phi_i} L_B = \mathbb{E}[(w_B^\top \Phi f - y_B) w_B f_i(x)].$$

Using the definitions of  $\Sigma^{(B)}$  and  $\beta^{(B)}$ :

$$\mathbb{E}[\nabla_{\phi_i} L_B] = \left( \sum_j \Sigma_{ij}^{(B)} \gamma_j^{(B)} - \beta_i^{(B)} \right) w_B, \quad \gamma_j^{(B)} := w_B^\top \phi_j.$$

Hence,

$$\mathbb{E}[\Delta \phi_i] = -\eta_\phi \left( \sum_j \Sigma_{ij}^{(B)} \gamma_j^{(B)} - \beta_i^{(B)} \right) w_B.$$

Finally, the total expected loss reduction under gradient descent is

$$\mathbb{E}[\Delta L_B] = \langle \nabla_{w_B} L_B, \Delta w_B \rangle + \sum_i \langle \nabla_{\phi_i} L_B, \Delta \phi_i \rangle = -\eta_w \|\nabla_{w_B} L_B\|^2 - \eta_\phi \sum_i \|\nabla_{\phi_i} L_B\|^2,$$

ignoring higher-order terms  $O(\eta^2)$ . This shows that loss reduction is shared between the two parameter groups in proportion to the squared gradient norms, yielding the load ratios  $\rho_w, \rho_\phi$ .  $\square$

**Corollary B.2** (Fixed-probe exaggerates forgetting). *The fixed-probe analysis presented in the main paper (Sec 3.3), which assumes  $w^{(B)}$  is fixed, overestimates the magnitude of first-order forgetting compared to a scenario with simultaneous probe and feature co-adaptation.*

Forgetting of task A manifests as readout misalignment and capacity degradation (via feature fading or overlap). Both are direct consequences of geometric transformations—scaling and rotation—applied to the feature vectors  $\phi_i$ . These transformations are driven by the gradient pressure on  $\Phi$  to reduce the error on task B.

1. **Fixed-Probe (Main Analysis):** In the fixed-probe setting, the readout  $w^{(B)}$  is frozen. To reduce the task B error, the gradient descent must apply *all* corrective pressure directly to the feature vectors  $\Phi$ . This forces the maximal amount of change onto  $\Phi$ , leading to larger, more destructive rotations and scaling of  $\phi_i$  vectors that may be important for task A.
2. **Co-adaptation (Proposition 1):** In the co-adaptation setting, the model can reduce the task B error by updating *both* the feature vectors  $\Phi$  and the probe  $w^{(B)}$ . The optimization finds a more efficient solution by "sharing the load." By allowing  $w^{(B)}$  to adapt, the model can correct for error by changing the reader, which in turn imposes less total gradient pressure on  $\Phi$  to change.

Because co-adaptation provides a "lower-cost" path to error reduction (by updating  $w^{(B)}$ ), it induces smaller and less destructive geometric transformations to  $\Phi$ . Smaller changes to the  $\phi_i$  vectors directly result in less capacity degradation (less fading and overlap) and less readout misalignment. Therefore, the fixed-probe analysis, which forces all change onto  $\Phi$ , models an exaggerated, worst-case scenario for feature vector disruption and thus overestimates both components of forgetting.

## C. Proof of theorem 3.3

*Proof.* We start from the per-example squared loss on task B,

$$\mathcal{L}_B(x) = \frac{1}{2} (\hat{y}^{(B)}(x) - y^{(B)}(x))^2, \quad \hat{y}^{(B)}(x) = w^{(B)\top} a_\ell(x).$$

By the chain rule for  $\phi_i$  (recall  $a_\ell(x) = \sum_j \phi_j f_j(x)$ ),

$$\nabla_{\phi_i} \mathcal{L}_B(x) = (\hat{y}^{(B)}(x) - y^{(B)}(x)) \nabla_{\phi_i} \hat{y}^{(B)}(x) = (\hat{y}^{(B)}(x) - y^{(B)}(x)) w^{(B)} f_i(x).$$

Next expand  $\hat{y}^{(B)}(x)$  using the feature decomposition:

$$\hat{y}^{(B)}(x) = w^{(B)\top} a_\ell(x) = \sum_j (w^{(B)\top} \phi_j) f_j(x).$$

Substitute this into the gradient expression:

$$\begin{aligned} \nabla_{\phi_i} \mathcal{L}_B(x) &= \left( \sum_j (w^{(B)\top} \phi_j) f_j(x) - y^{(B)}(x) \right) w^{(B)} f_i(x) \\ &= (w^{(B)\top} \phi_i) f_i(x)^2 w^{(B)} + \left( \sum_{j \neq i} (w^{(B)\top} \phi_j) f_j(x) \right) f_i(x) w^{(B)} - y^{(B)}(x) f_i(x) w^{(B)}. \end{aligned}$$

Take expectation over  $x \sim \mathcal{D}_B$ . Group terms and use linearity:

$$\begin{aligned} \mathbb{E}_{\mathcal{D}_B} [\nabla_{\phi_i} \mathcal{L}_B] &= (w^{(B)\top} \phi_i) \mathbb{E}[f_i(x)^2] w^{(B)} + \sum_{j \neq i} (w^{(B)\top} \phi_j) \mathbb{E}[f_j(x) f_i(x)] w^{(B)} \\ &\quad - \mathbb{E}[y^{(B)}(x) f_i(x)] w^{(B)}. \end{aligned}$$

Substitute the definitions  $\gamma_j^{(B)} = w^{(B)\top} \phi_j$ ,  $\Sigma_{ij}^{(B)} = \mathbb{E}[f_i f_j]$ , and  $\beta_i^{(B)} = \mathbb{E}[y^{(B)} f_i]$  to obtain

$$\mathbb{E}_{\mathcal{D}_B} [\nabla_{\phi_i} \mathcal{L}_B] = \left( \sum_j \gamma_j^{(B)} \Sigma_{ij}^{(B)} - \beta_i^{(B)} \right) w^{(B)}.$$

Finally, a gradient-descent step with step size  $\eta$  updates  $\phi_i$  by

$$\Delta \phi_i = -\eta \mathbb{E}_{\mathcal{D}_B} [\nabla_{\phi_i} \mathcal{L}_B] = -\eta \left( \sum_j \gamma_j^{(B)} \Sigma_{ij}^{(B)} - \beta_i^{(B)} \right) w^{(B)},$$

which is equation 8.  $\square$

## D. Extended analysis of feature updates

### D.1. Feature updates with shared probes

The main analysis focuses on the case where a different probe is used at each task. Here, we extend the analysis to the case in which all probes are shared across tasks. When focusing on the penultimate layer, this corresponds to a **class-incremental learning (CIL)** setting with a shared classifier over all classes.

We assume that the two adjacent tasks  $A$  and  $B$  contain samples from disjoint class sets. For each class  $c$ , samples belonging to that class have a nonzero target  $y_c(\mathbf{x}) \neq 0$ , while samples from other classes have target  $y_c(\mathbf{x}) = 0$ . Importantly, old classes are not masked during training on task  $B$ ; instead, they receive zero targets.

Under this setup, gradient descent on task  $B$  induces an additional data-dependent term on the feature vectors, arising from classes in previous tasks. This term depends on feature correlations under  $\mathcal{D}_B$  and on the alignment between features and old class probes, and acts to reduce the contribution of features to old class predictions. In other words, **this additional term acts as a suppressive pressure on features predictive of Task A classes and activated under  $\mathcal{D}_B$** . Formally:

**Lemma D.1** (Expected feature vector update during Task  $B$  training with shared probes). *Let  $\mathcal{C}_A$  and  $\mathcal{C}_B$  be disjoint sets of classes, where  $\mathcal{C}_A$  was learned previously in Task  $A$ . Let the shared probe matrix be  $W = [w_1, w_2, \dots, w_K]$ . Under Task  $B$  training ( $\mathbf{x} \sim \mathcal{D}_B$ ), no classes from Task  $A$  appear and thus the targets for Task  $A$  classes are strictly zero:  $y_c^{(B)}(\mathbf{x}) = 0$  for all  $c \in \mathcal{C}_A$ .*

Define the feature correlation as  $\Sigma_{i,j}^{(B)} := \mathbb{E}_{\mathbf{x} \sim \mathcal{D}_B} [f_i(\mathbf{x}) f_j(\mathbf{x})]$ , the probe sensitivity as  $\gamma_{j,c} := w_c^\top \phi_j$ , and the feature contribution as  $\beta_{i,c}^{(B)} := \mathbb{E}_{\mathbf{x} \sim \mathcal{D}_B} [y_c^{(B)}(\mathbf{x}) f_i(\mathbf{x})]$ .

The expected gradient-descent update on feature vector  $\phi_i$  during Task B is:

$$\mathbb{E}_{\mathbf{x} \sim \mathcal{D}_B} [\Delta \phi_i] = -\eta \left[ \underbrace{\sum_{c \in \mathcal{C}_B} \left( \sum_j \gamma_{j,c} \Sigma_{ij}^{(B)} - \beta_{i,c}^{(B)} \right) w_c}_{\text{Task B Learning}} + \underbrace{\sum_{c \in \mathcal{C}_A} \left( \sum_j \gamma_{j,c} \Sigma_{ij}^{(B)} \right) w_c}_{\text{Task A Suppression}} \right]. \quad (14)$$

*Proof.* We define the per-example squared loss across all  $K$  classes for Task B as:

$$\mathcal{L}_B(\mathbf{x}) = \frac{1}{2} \sum_{c=1}^K (\hat{y}_c(\mathbf{x}) - y_c^{(B)}(\mathbf{x}))^2, \quad \hat{y}_c(\mathbf{x}) = w_c^\top a_\ell(\mathbf{x}).$$

By the chain rule, the gradient with respect to  $\phi_i$  is obtained by summing the contribution from each class output. Since  $a_\ell(\mathbf{x}) = \sum_j \phi_j f_j(\mathbf{x})$ , we have  $\nabla_{\phi_i} \hat{y}_c(\mathbf{x}) = w_c f_i(\mathbf{x})$ . Therefore:

$$\nabla_{\phi_i} \mathcal{L}_B(\mathbf{x}) = \sum_{c=1}^K (\hat{y}_c(\mathbf{x}) - y_c^{(B)}(\mathbf{x})) w_c f_i(\mathbf{x}).$$

Expanding  $\hat{y}_c(\mathbf{x}) = \sum_j (w_c^\top \phi_j) f_j(\mathbf{x}) = \sum_j \gamma_{j,c} f_j(\mathbf{x})$  and distributing  $f_i(\mathbf{x}) w_c$ :

$$\begin{aligned} \nabla_{\phi_i} \mathcal{L}_B(\mathbf{x}) &= \sum_{c=1}^K \left( \sum_j \gamma_{j,c} f_j(\mathbf{x}) - y_c^{(B)}(\mathbf{x}) \right) w_c f_i(\mathbf{x}) \\ &= \sum_{c=1}^K \left( \sum_j \gamma_{j,c} f_j(\mathbf{x}) f_i(\mathbf{x}) - y_c^{(B)}(\mathbf{x}) f_i(\mathbf{x}) \right) w_c. \end{aligned}$$

Taking the expectation over  $\mathbf{x} \sim \mathcal{D}_B$  and applying linearity of expectation:

$$\mathbb{E}_{\mathbf{x} \sim \mathcal{D}_B} [\nabla_{\phi_i} \mathcal{L}_B(\mathbf{x})] = \sum_{c=1}^K \left( \sum_j \gamma_{j,c} \Sigma_{ij}^{(B)} - \beta_{i,c}^{(B)} \right) w_c,$$

where we have used the definitions  $\Sigma_{ij}^{(B)} = \mathbb{E}_{\mathbf{x} \sim \mathcal{D}_B} [f_i(\mathbf{x}) f_j(\mathbf{x})]$  and  $\beta_{i,c}^{(B)} = \mathbb{E}_{\mathbf{x} \sim \mathcal{D}_B} [y_c^{(B)}(\mathbf{x}) f_i(\mathbf{x})]$ .

Since we are training on Task B, the labels for previously learned Task A classes are zero:  $y_c^{(B)}(\mathbf{x}) = 0$  for all  $c \in \mathcal{C}_A$ . Consequently,  $\beta_{i,c}^{(B)} = \mathbb{E}_{\mathbf{x} \sim \mathcal{D}_B} [0 \cdot f_i(\mathbf{x})] = 0$  for  $c \in \mathcal{C}_A$ .

Partitioning the sum over all  $K$  classes into  $\mathcal{C}_B$  and  $\mathcal{C}_A$ :

$$\begin{aligned} \mathbb{E}_{\mathbf{x} \sim \mathcal{D}_B} [\nabla_{\phi_i} \mathcal{L}_B(\mathbf{x})] &= \sum_{c \in \mathcal{C}_B} \left( \sum_j \gamma_{j,c} \Sigma_{ij}^{(B)} - \beta_{i,c}^{(B)} \right) w_c \\ &\quad + \sum_{c \in \mathcal{C}_A} \left( \sum_j \gamma_{j,c} \Sigma_{ij}^{(B)} - 0 \right) w_c. \end{aligned}$$

The gradient-descent update with learning rate  $\eta$  is

$$\mathbb{E}_{\mathbf{x} \sim \mathcal{D}_B} [\Delta \phi_i] = -\eta \mathbb{E}_{\mathbf{x} \sim \mathcal{D}_B} [\nabla_{\phi_i} \mathcal{L}_B(\mathbf{x})],$$

which yields equation equation 14.  $\square$

Equation equation 14 isolates the mechanism of feature forgetting with shared probes: the second summation acts as a suppressive term, actively suppressing any features aligned with Task A probes to satisfy the  $y_c^{(B)} = 0$  targets. In a

fixed-probe scenario (as in the main analysis), the feature matrix  $\Phi$  must absorb the entirety of this suppression load, placing the full burden of this suppressive pressure on the feature representations. However, as discussed in section B, under simultaneous probe co-adaptation, the Task A weight vectors  $w_c$  (for  $c \in \mathcal{C}_A$ ) also update, naturally decaying or rotating away from the active Task B features. By sharing this gradient load, the degradation of the old classifier weights reduces the impact of optimization on underlying features. Thus, while fixed-probe analysis is useful for isolating feature dynamics, it represents a worst-case scenario that overestimates the magnitude of representation degradation.

## D.2. Feature updates under cross-entropy loss

We now extend the analysis to the standard classification setting using the cross-entropy (CE) loss with a softmax activation, to better understand how a different loss function affects the results in the penultimate layer of a model.

We define the per-example CE loss as  $\mathcal{L}_{CE}(\mathbf{x}) = -\sum_{c=1}^K y_c^{(B)}(\mathbf{x}) \log p_c(\mathbf{x})$ , where the class probability  $p_c(\mathbf{x})$  is given by the softmax of the logits:

$$p_c(\mathbf{x}) = \frac{\exp(w_c^\top a_\ell(\mathbf{x}))}{\sum_{k=1}^K \exp(w_k^\top a_\ell(\mathbf{x}))}. \quad (15)$$

Recall that for Task B samples, targets for Task A classes are zero:  $y_c^{(B)}(\mathbf{x}) = 0$  for all  $c \in \mathcal{C}_A$ . Taking the expectation over  $\mathcal{D}_B$ , the update rule becomes:

**Lemma D.2** (Feature vector update under cross-entropy). *Let the loss function be the cross-entropy loss  $\mathcal{L}_{CE}(\mathbf{x}) = -\sum_{k=1}^K y_k^{(B)}(\mathbf{x}) \log p_k(\mathbf{x})$ , where  $p_k(\mathbf{x})$  is the softmax output. Under the same task setup as theorem D.1 (disjoint class sets with zero targets for old classes  $c \in \mathcal{C}_A$ ), the expected update for feature vector  $\phi_i$  is:*

$$\mathbb{E}_{\mathbf{x} \sim \mathcal{D}_B} [\Delta \phi_i] = -\eta \left[ \sum_{c \in \mathcal{C}_B} \left( \mathbb{E}_{\mathbf{x} \sim \mathcal{D}_B} [p_c(\mathbf{x}) f_i(\mathbf{x})] - \beta_{i,c}^{(B)} \right) w_c + \sum_{c \in \mathcal{C}_A} \left( \mathbb{E}_{\mathbf{x} \sim \mathcal{D}_B} [p_c(\mathbf{x}) f_i(\mathbf{x})] \right) w_c \right]. \quad (16)$$

*Proof.* The gradient of the cross-entropy loss with respect to the logit  $\hat{y}_c(\mathbf{x})$  is the standard softmax error signal:

$$\frac{\partial \mathcal{L}_{CE}(\mathbf{x})}{\partial \hat{y}_c(\mathbf{x})} = p_c(\mathbf{x}) - y_c^{(B)}(\mathbf{x}).$$

Recall that the logit decomposes as  $\hat{y}_c(\mathbf{x}) = w_c^\top a_\ell(\mathbf{x}) = w_c^\top \sum_j \phi_j f_j(\mathbf{x})$ . The gradient of  $\hat{y}_c(\mathbf{x})$  with respect to the feature vector  $\phi_i$  is:

$$\nabla_{\phi_i} \hat{y}_c(\mathbf{x}) = w_c f_i(\mathbf{x}).$$

Applying the chain rule and summing over all  $K$  classes:

$$\begin{aligned} \nabla_{\phi_i} \mathcal{L}_{CE}(\mathbf{x}) &= \sum_{c=1}^K \frac{\partial \mathcal{L}_{CE}(\mathbf{x})}{\partial \hat{y}_c(\mathbf{x})} \cdot \nabla_{\phi_i} \hat{y}_c(\mathbf{x}) \\ &= \sum_{c=1}^K (p_c(\mathbf{x}) - y_c^{(B)}(\mathbf{x})) w_c f_i(\mathbf{x}). \end{aligned}$$

Taking the expectation over the data distribution  $\mathcal{D}_B$  and partitioning the sum into current task classes  $\mathcal{C}_B$  and old task classes  $\mathcal{C}_A$ :

For current task classes ( $c \in \mathcal{C}_B$ ):

$$\mathbb{E}_{\mathbf{x} \sim \mathcal{D}_B} \left[ (p_c(\mathbf{x}) - y_c^{(B)}(\mathbf{x})) f_i(\mathbf{x}) \right] w_c = \left( \mathbb{E}_{\mathbf{x} \sim \mathcal{D}_B} [p_c(\mathbf{x}) f_i(\mathbf{x})] - \beta_{i,c}^{(B)} \right) w_c,$$

where we used the definition  $\beta_{i,c}^{(B)} = \mathbb{E}_{\mathbf{x} \sim \mathcal{D}_B} [y_c^{(B)}(\mathbf{x}) f_i(\mathbf{x})]$ .

For old task classes ( $c \in \mathcal{C}_A$ ), the targets are zero:  $y_c^{(B)}(\mathbf{x}) = 0$ . Thus:

$$\mathbb{E}_{\mathbf{x} \sim \mathcal{D}_B} \left[ (p_c(\mathbf{x}) - 0) f_i(\mathbf{x}) \right] w_c = \mathbb{E}_{\mathbf{x} \sim \mathcal{D}_B} [p_c(\mathbf{x}) f_i(\mathbf{x})] w_c.$$

The gradient descent update  $\mathbb{E}_{\mathbf{x} \sim \mathcal{D}_B} [\Delta \phi_i] = -\eta \mathbb{E}_{\mathbf{x} \sim \mathcal{D}_B} [\nabla_{\phi_i} \mathcal{L}_{CE}(\mathbf{x})]$  yields equation equation 16.  $\square$

Equation equation 16 preserves the structural form of the MSE update in theorem D.1. The first summation drives alignment with the new task (incorporating the feature contribution  $\beta_{i,c}^{(B)}$ ), while the second summation acts as the suppressive pressure from old tasks. Note, however, that under CE, feature correlations are implicit via  $p_c(\mathbf{x})$ , and suppression depends on the full logit distribution through the softmax.

The nature of the suppression, however, differs fundamentally. In the linear MSE case, the suppressive term depends on the raw logits ( $\hat{y}_c(\mathbf{x})$ ), scaling linearly with feature activations through  $\sum_j \gamma_{j,c} \Sigma_{ij}^{(B)}$ . Under CE, the suppressive term for an old class  $c \in \mathcal{C}_A$  is weighted by the predicted probability  $p_c(\mathbf{x})$ . Consequently, suppressive pressure in CE is dynamic and probability-modulated: it is strong only when a Task  $B$  sample is "confused" for an old class (i.e., when  $p_c(\mathbf{x})$  is non-negligible). If the new task features are approximately orthogonal to the old class probes, or if the model is confident in its Task  $B$  predictions, then  $p_c(\mathbf{x}) \rightarrow 0$  for  $c \in \mathcal{C}_A$ , and the suppressive gradient becomes negligible. This suggests that **CE loss may offer a milder form of feature forgetting compared to MSE**, provided the classes are sufficiently separable in the representation space and the model maintains high confidence on new task predictions.

## E. Proof of theorem 3.4

*Proof. Context & Definitions.* Before starting, let's define the terms based on the loss function:

- $\mathcal{L}^{(A)}(\Phi) := \frac{1}{2} \mathbb{E}[(w^{(A)\top} \Phi f^{(A)} - y^{(A)})^2]$
- $\Sigma^{(A)} := \mathbb{E}[f^{(A)} f^{(A)\top}]$  is the covariance matrix of features  $f^{(A)}$ .
- We assume  $\mathbb{E}[y^{(A)2}] = 1$ .
- $\dagger$  denotes the Moore-Penrose pseudoinverse.

**1. Task  $A$  expected loss.** We expand the expectation and substitute following the definitions  $\beta^{(A)} := \mathbb{E}[f^{(A)} y^{(A)}]$  and  $\Sigma^{(A)} := \mathbb{E}[f^{(A)} f^{(A)\top}]$ .

$$\begin{aligned} \mathcal{L}^{(A)}(\Phi) &= \frac{1}{2} \mathbb{E}[(w^{(A)\top} \Phi f^{(A)})^2 - 2(w^{(A)\top} \Phi f^{(A)}) y^{(A)} + (y^{(A)})^2] \\ &= \frac{1}{2} \left( \mathbb{E}[(w^{(A)\top} \Phi f^{(A)}) (f^{(A)\top} \Phi^\top w^{(A)})] - 2\mathbb{E}[w^{(A)\top} \Phi f^{(A)} y^{(A)}] + \mathbb{E}[y^{(A)2}] \right) \\ &= \frac{1}{2} \left( w^{(A)\top} \Phi \mathbb{E}[f^{(A)} f^{(A)\top}] \Phi^\top w^{(A)} - 2w^{(A)\top} \Phi \mathbb{E}[f^{(A)} y^{(A)}] + 1 \right) \\ &= \frac{1}{2} \left( (w^{(A)\top} \Phi \Sigma^{(A)} \Phi^\top w^{(A)} - 2(w^{(A)\top} \Phi \beta^{(A)} + 1) \right) \end{aligned}$$

**2. Loss at the task- $A$  optimum.** To find the optimum, we simplify the problem. Let  $z = \Phi^\top w^{(A)}$ . The loss becomes a quadratic function of  $z$ :

$$\mathcal{L}^{(A)}(z) = \frac{1}{2} (z^\top \Sigma^{(A)} z - 2z^\top \beta^{(A)} + 1)$$

We find the minimum by setting the gradient with respect to  $z$  to zero:

$$\nabla_z \mathcal{L}^{(A)}(z) = \Sigma^{(A)} z - \beta^{(A)} = 0$$

The (minimal-norm) solution  $z_{\text{opt}}$  that satisfies this first-order condition is:

$$z_{\text{opt}} = (\Sigma^{(A)})^\dagger \beta^{(A)}$$

Now, we plug  $z_{\text{opt}}$  back into the loss. We use the property  $(\Sigma^{(A)})^\dagger \Sigma^{(A)} (\Sigma^{(A)})^\dagger = (\Sigma^{(A)})^\dagger$ :

$$\begin{aligned} \mathcal{L}^{(A)}(\Phi_{\text{opt}}^{(A)}) &= \mathcal{L}^{(A)}(z_{\text{opt}}) = \frac{1}{2} (z_{\text{opt}}^\top \Sigma^{(A)} z_{\text{opt}} - 2z_{\text{opt}}^\top \beta^{(A)} + 1) \\ &= \frac{1}{2} \left( ((\Sigma^{(A)})^\dagger \beta^{(A)})^\top \Sigma^{(A)} ((\Sigma^{(A)})^\dagger \beta^{(A)}) - 2((\Sigma^{(A)})^\dagger \beta^{(A)})^\top \beta^{(A)} + 1 \right) \\ &= \frac{1}{2} \left( \beta^{(A)\top} (\Sigma^{(A)})^\dagger \Sigma^{(A)} (\Sigma^{(A)})^\dagger \beta^{(A)} - 2\beta^{(A)\top} (\Sigma^{(A)})^\dagger \beta^{(A)} + 1 \right) \\ &= \frac{1}{2} \left( \beta^{(A)\top} (\Sigma^{(A)})^\dagger \beta^{(A)} - 2\beta^{(A)\top} (\Sigma^{(A)})^\dagger \beta^{(A)} + 1 \right) \\ &= \frac{1}{2} (1 - \beta^{(A)\top} (\Sigma^{(A)})^\dagger \beta^{(A)}) \end{aligned}$$

**3. Minimal-norm solution for task  $B$ .** This step defines the optimal solution for task  $B$ . The optimal solution satisfies  $\Phi^\top w^{(B)} = v$ , where  $v = (\Sigma^{(B)})^\dagger \beta^{(B)}$ . We are given the minimal Frobenius norm solution  $\Phi_{\text{opt}}^{(B)} = \frac{w^{(B)} v^\top}{\|w^{(B)}\|^2}$ . We compute  $z_B = \Phi_{\text{opt}}^{(B)\top} w^{(A)}$ . Let  $\alpha := \frac{w^{(B)\top} w^{(A)}}{\|w^{(B)}\|^2}$ .

$$\begin{aligned}\Phi_{\text{opt}}^{(B)\top} w^{(A)} &= \left( \frac{w^{(B)} v^\top}{\|w^{(B)}\|^2} \right)^\top w^{(A)} = \frac{(v^\top)^\top (w^{(B)})^\top}{\|w^{(B)}\|^2} w^{(A)} \\ &= \frac{v (w^{(B)\top} w^{(A)})}{\|w^{(B)}\|^2} = v \left( \frac{w^{(B)\top} w^{(A)}}{\|w^{(B)}\|^2} \right) = \alpha v\end{aligned}$$

**4. Evaluate task  $A$  loss at  $\Phi_{\text{opt}}^{(B)}$ .** We evaluate the task  $A$  loss using  $\mathcal{L}^{(A)}(z)$  from Step 2, with  $z_B = \Phi_{\text{opt}}^{(B)\top} w^{(A)} = \alpha v$ .

$$\begin{aligned}\mathcal{L}^{(A)}(\Phi_{\text{opt}}^{(B)}) &= \mathcal{L}^{(A)}(z_B) = \frac{1}{2} (z_B^\top \Sigma^{(A)} z_B - 2z_B^\top \beta^{(A)} + 1) \\ &= \frac{1}{2} ((\alpha v)^\top \Sigma^{(A)} (\alpha v) - 2(\alpha v)^\top \beta^{(A)} + 1) \\ &= \frac{1}{2} (\alpha^2 v^\top \Sigma^{(A)} v - 2\alpha v^\top \beta^{(A)} + 1)\end{aligned}$$

**5. Exact loss change.** We compute  $\Delta \mathcal{L}^{(A)} = \mathcal{L}^{(A)}(\Phi_{\text{opt}}^{(B)}) - \mathcal{L}^{(A)}(\Phi_{\text{opt}}^{(A)})$ .

$$\begin{aligned}\Delta \mathcal{L}^{(A)} &= \frac{1}{2} (\alpha^2 v^\top \Sigma^{(A)} v - 2\alpha v^\top \beta^{(A)} + 1) - \frac{1}{2} (1 - \beta^{(A)\top} (\Sigma^{(A)})^\dagger \beta^{(A)}) \\ &= \frac{1}{2} (\alpha^2 v^\top \Sigma^{(A)} v - 2\alpha v^\top \beta^{(A)} + 1 - 1 + \beta^{(A)\top} (\Sigma^{(A)})^\dagger \beta^{(A)}) \\ &= \frac{1}{2} (\alpha^2 v^\top \Sigma^{(A)} v - 2\alpha v^\top \beta^{(A)} + \beta^{(A)\top} (\Sigma^{(A)})^\dagger \beta^{(A)})\end{aligned}$$

This equals  $\frac{1}{2} (\alpha v - (\Sigma^{(A)})^\dagger \beta^{(A)})^\top \Sigma^{(A)} (\alpha v - (\Sigma^{(A)})^\dagger \beta^{(A)})$ . We verify by expanding:

$$\begin{aligned}&\frac{1}{2} (\alpha v - (\Sigma^{(A)})^\dagger \beta^{(A)})^\top \Sigma^{(A)} (\alpha v - (\Sigma^{(A)})^\dagger \beta^{(A)}) \\ &= \frac{1}{2} ((\alpha v)^\top \Sigma^{(A)} (\alpha v) - 2(\alpha v)^\top \Sigma^{(A)} ((\Sigma^{(A)})^\dagger \beta^{(A)}) + ((\Sigma^{(A)})^\dagger \beta^{(A)})^\top \Sigma^{(A)} ((\Sigma^{(A)})^\dagger \beta^{(A)})) \\ &= \frac{1}{2} (\alpha^2 v^\top \Sigma^{(A)} v - 2\alpha v^\top (\Sigma^{(A)} (\Sigma^{(A)})^\dagger \beta^{(A)}) + \beta^{(A)\top} (\Sigma^{(A)})^\dagger \Sigma^{(A)} (\Sigma^{(A)})^\dagger \beta^{(A)}) \\ &= \frac{1}{2} (\alpha^2 v^\top \Sigma^{(A)} v - 2\alpha v^\top (\Sigma^{(A)} (\Sigma^{(A)})^\dagger \beta^{(A)}) + \beta^{(A)\top} (\Sigma^{(A)})^\dagger \beta^{(A)})\end{aligned}$$

This matches our expression for  $\Delta \mathcal{L}^{(A)}$  under the assumption that  $\beta^{(A)}$  is in the column space of  $\Sigma^{(A)}$ , which implies  $\Sigma^{(A)} (\Sigma^{(A)})^\dagger \beta^{(A)} = \beta^{(A)}$ .  $\square$

## F. Full experimental setup of the encoder-reader model

### F.1. Feature-reader Model Details

We implemented the feature-reader model in PyTorch (Imambi et al., 2021). The model consists of a shared 1-layer encoder,  $\Phi$ , which maps 80 features to 20 activation dimensions, and five task-specific linear heads ( $w_t$ ).

- **Task definition:** Each task is defined by a unique contribution vector,  $\beta_t$ , which specifies a sparse subset of features relevant to that task.  $\beta_t$  is randomly sampled from a standard normal distribution.
- **Data generation:** We generated 20,000 synthetic data samples by sampling feature activations uniformly in the range  $[0, 1]$  with 90% sparsity (feature  $i$  is 0 with a probability of 90%). In the ‘none’ scenario, this was followed by masking out features from other tasks.
- **Training:** The model was trained sequentially on five tasks using batch gradient descent with the Adam optimizer and  $lr = 0.01$ . We minimized the Mean Squared Error (MSE) loss. We trained the model for 10,000 epochs at each task to ensure convergence. All results reported are the average of 5 independent seeds.

## F.2. Forgetting Metric (F) Formulation

To quantify forgetting, we measure the degradation of a given metric (e.g., accuracy, normalized capacity) for all previously learned tasks.

For any task  $i$  and any subsequent task  $t$  (where  $t > i$ ), we first compute the relative performance ratio,  $R_{i,t}$ :

$$R_{i,t} = \frac{M_{i,t}}{M_{i,i}}, \quad (17)$$

where  $M_{i,i}$  is the value of the metric for task  $i$  immediately after it was trained and  $M_{i,t}$  is the value of the same metric for task  $i$  after the model has finished training on task  $t$ .

The forgetting value for task  $i$  is  $1 - R_{i,t}$ . A value of 1 indicates complete forgetting, meaning the metric's value has dropped to zero relative to its original level.

The final **forgetting (F)** score reported in our plots at step  $t$  is the average forgetting across all previously learned tasks  $i < t$ :

$$F = \frac{1}{t-1} \sum_{i=1}^{t-1} (1 - R_{i,t}). \quad (18)$$

Before this calculation, all metrics are first averaged over the features associated with a specific task.

## G. Introduction to crosscoders

### G.1. Sparse Autoencoders

The linear representation hypothesis (Equation (1)) posits that features are encoded as directions in activation space, while the superposition hypothesis suggests the number of underlying features exceeds the neuron count ( $d_{\text{model}}$ ), making features difficult to disentangle.

*Sparse Autoencoders (SAEs)* are employed to *decouple* these superposed features and uncover the individual features learned by a neural network. An SAE maps a layer representation  $a_\ell(x) \in \mathbb{R}^{d_{\text{model}}}$  to a *higher-dimensional, sparse latent space* ( $d_{\text{cross}} > d_{\text{model}}$ ). In this latent space, each dimension is encouraged to be *monosemantic*, corresponding to a single feature.

The SAE operates via an encoding-decoding process:

$$f_{\text{enc}}(x) = g(\mathbf{W}_{\text{enc}} a_\ell(x) + b_{\text{enc}}) \quad (19)$$

$$\text{SAE}(x) = \mathbf{W}_{\text{dec}} f_{\text{enc}}(x) + b_{\text{dec}} \quad (20)$$

where  $\mathbf{W}_{\text{enc}} \in \mathbb{R}^{d_{\text{cross}} \times d_{\text{model}}}$  and  $\mathbf{W}_{\text{dec}} \in \mathbb{R}^{d_{\text{model}} \times d_{\text{cross}}}$  are the learnable encoder and decoder matrices (the *dictionary*), respectively. The encoder produces feature activations  $f_{\text{enc}}(x) \in \mathbb{R}^{d_{\text{cross}}}$ , using ReLU and TopK activation functions  $g(\cdot)$  (Gao et al., 2025).

SAEs are trained to accurately reconstruct the original representation  $a_\ell(x)$  while enforcing  $\ell_1$  *sparsity* on the feature activations. The loss function defines this:

$$\mathcal{L}(x) = \|a_\ell(x) - \text{SAE}(x)\|_2 + \alpha \|f_{\text{enc}}(x)\|_1. \quad (21)$$

The sparsity constraint ensures that, once trained,  $a_\ell(x)$  is approximated as a *sparse linear combination* of the columns of the learned dictionary  $\mathbf{W}_{\text{dec}}$ , from which interpretable and monosemantic features are often extracted (Bricken et al., 2023; Huben et al., 2024).

**SAEs and our conceptual framework** We use SAEs to extend the feature analysis to larger neural networks. The components of the trained SAE directly map to the concepts in our framework:

- The  $i$ -th component of the feature activation,  $f_{\text{enc},i}(x)$ , is interpreted as the feature activation  $f_i(x)$ .

- The  $i$ -th column of the decoder matrix,  $\mathbf{W}_{\text{dec},i}$ , is analogous to the feature vector  $\phi_i$ , as it defines feature  $i$ 's contribution to the reconstructed activation.

## G.2. Crosscoders

*Crosscoders* (Lindsey et al., 2024) are a specialized variant of SAEs designed to study features encoded across multiple layers and for *model diffing*, which is the study of how different models encode features. This approach is particularly valuable for analyzing sequential changes, such as in a *continual learning setup* with a set of models  $\mathcal{M} = \{m_1, m_2, \dots, m_T\}$ , corresponding to models trained on  $T$  sequential tasks. The core distinction of a crosscoder is the *shared encoding step*. Representations from different models  $a_\ell^{m_t}(x)$  (at layer  $\ell$  for model  $m_t$ ) for the same input  $x$  are aggregated and mapped into a *single, shared latent feature space*:

$$f_{\text{enc}}(x) = g\left(\sum_{m_t \in \mathcal{M}} \mathbf{W}_{\text{enc}}^{m_t} a_\ell^{m_t}(x) + b_{\text{enc}}\right), \quad (22)$$

with  $\mathbf{W}_{\text{enc}}^{m_t}$  and  $b_{\text{enc}}$  denoting the encoder weights for model  $m_t$ , and  $a_\ell^{m_t}$  the representation of model  $m_t$  at layer  $\ell$ . The decoding step uses individual decoders to reconstruct each model's original representation from the shared activations:

$$\text{CROSS}^{m_t}(a_\ell^{m_t}(x)) = \mathbf{W}_{\text{dec}}^{m_t} f_{\text{enc}}(x) + b_{\text{dec}}^{m_t}, \quad (23)$$

where  $b_{\text{dec}}^{m_t}$  is the corresponding model-specific bias. A schematic overview of the process is provided in Figure 5. The training objective is a combination of reconstruction loss and a regularization term:

$$\mathcal{L}(x) = \sum_{m_t \in \mathcal{M}} \|a_\ell^{m_t}(x) - \text{CROSS}^{m_t}(a_\ell^{m_t}(x))\|_2 + \lambda \sum_i f_{\text{enc}_i}(x) \sum_{m_t \in \mathcal{M}} \|\mathbf{W}_{\text{dec},i}^{m_t}\|. \quad (24)$$

The second term,  $\lambda \sum_i f_{\text{enc}_i}(x) \sum_{m_t \in \mathcal{M}} \|\mathbf{W}_{\text{dec},i}^{m_t}\|_2$ , encourages feature compression. It pushes the decoder weights for feature  $i$  ( $\mathbf{W}_{\text{dec},i}^{m_t}$ ) toward zero norm if feature  $i$  is inactive or non-shared across a subset of models. This regularization helps *isolate features* that are unique to certain models or tasks.

**Application to continual learning** In the context of this work, the crosscoder analysis enables us to study the **evolution** of the decoder vector  $\mathbf{W}_{\text{dec},i}^{m_t}$  across sequential tasks  $m_t$ . Similar to the analysis of the feature vector  $\phi_i$  in the conceptual framework (Section 3), we can track the transformation of features and the allocation of feature capacity across the continual learning process.

## H. Setup for the ViT and crosscoder experiment

This section outlines the experimental setup for the continual learning experiments on the CIFAR-10 dataset, including the Vision Transformer (ViT) and Top-K Sparse Autoencoder (TopKSAE) training procedures.

### H.1. Dataset and Task Protocol

We use the CIFAR-10 dataset, which consists of 60,000 32x32 color images in 10 classes, partitioned into a 50,000-image training set and a 10,000-image test set. For our experiments, all images are resized to 224x224.

For our continual learning benchmark, we use the **Split CIFAR-10** protocol. The 10 classes of CIFAR-10 are split into 5 sequential tasks, with each task containing 2 distinct classes. The model is trained sequentially on these tasks. The specific class sequence used for the experiments is:

- **Task 1:** Classes {5, 9} (dog, truck)
- **Task 2:** Classes {3, 1} (cat, automobile)
- **Task 3:** Classes {7, 2} (horse, bird)

- **Task 4:** Classes {6, 4} (frog, deer)
- **Task 5:** Classes {0, 8} (airplane, ship)

## H.2. Vision Transformer (ViT) Training

### H.2.1. MODEL ARCHITECTURE

Our base model is a Vision Transformer (ViT) with the following architecture:

- **Image Size:** 224x224
- **Patch Size:** 16x16
- **Embedding Dimension (hidden\_size):** 128
- **Number of Layers (Depth):** 6
- **Number of Attention Heads:** 4
- **MLP Dimension (intermediate\_size):** 256
- **Output Head:** A separate linear layer is trained for each task, mapping the final [CLS] token representation to the 2 classes of that task.

### H.2.2. TRAINING SETUP

The model is trained on each of the 5 tasks sequentially using a standard fine-tuning approach. For each new task, the model weights are initialized from the checkpoint of the previous task, and a new classification head is trained.

- **Optimizer:** Adam
- **Learning Rate:** 1e-4
- **Weight Decay:** 0.0
- **Batch Size:** 128
- **Epochs per Task:** 100
- **Learning Rate Scheduler:** Cosine Annealing

## H.3. Top-K Sparse Autoencoder (TopKSAE) Setup

We train and apply Top-K Sparse Autoencoders (which we refer to as "crosscoders") to the token activations of the ViT.

### H.3.1. TRAINING

The TopK SAEs are trained only once after the completion of the last task. They are trained on activations extracted from the ViT using the full training data from all tasks.

- **Target Layers:** We train separate SAEs for the outputs of the final, third-to-last, and sixth-to-last transformer blocks (corresponding to layers -1, -3, and -6).
- **SAE Architecture:**
  - **Dictionary Size (nb\_concepts):** 192 (calculated as  $d_{model} * 1.5$ )
  - **Sparsity:** We use a Top-K activation function with a **sparse factor of 6**, retaining only the six largest feature activations and setting all others to zero.
- **SAE Training Hyperparameters:**

- **Optimizer:** Adam
- **Learning Rate:** 5e-4
- **Batch Size:** 256
- **Epochs:** 3
- **L1 Regularization:** max coefficient of 0.001, linearly warmed up over the first 5% of training

#### H.4. Reproducibility

All experiments were conducted across **4 different random seeds** to ensure the robustness of our findings. The code will be made public upon publication.

### I. Feature visualizations across tasks

We visualize the activation maps of the top five important features of task 1 across all tasks for each layer. Feature IDs are layer-specific and not shared across layers. The activation maps highlight the image regions where the feature activates. Many features appear to correspond to confounders, such as asphalt (fig. 10, first row) or grass (fig. 11, first row), and these activations remain consistent across tasks, matching the worst-case scenario in section 3.3. Features in shallower layers tend to be less interpretable (fig. 12). Overall, this qualitative analysis illustrates how crosscoders can be used to probe model representations, including the identification of confounding features.



Figure 10. Activation maps for the top-5 (descending order) most important features in task 1 across tasks for layer -1. Shown are the images that most strongly activated each feature at each task. We overlay the images with their corresponding activation maps.



Figure 11. Activation maps for the top-5 (descending order) most important features in task 1 across tasks for layer -3. Shown are the images that most strongly activated each feature at each task. We overlay the images with their corresponding activation maps.

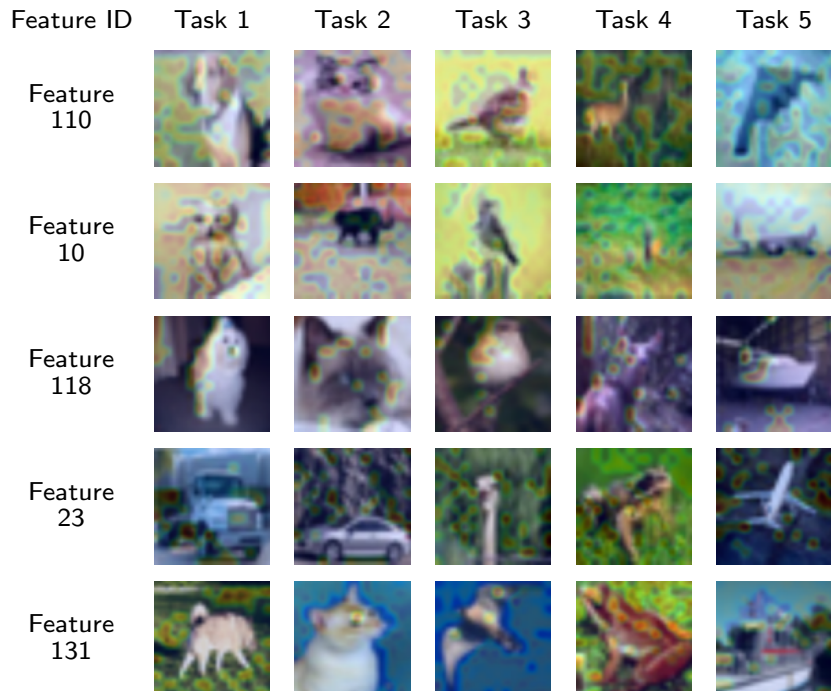


Figure 12. Activation maps for the top-5 (descending order) most important features in task 1 across tasks for layer -6. Shown are the images that most strongly activated each feature at each task. We overlay the images with their corresponding activation maps.

## J. Repeated features across layers

In Figure 13 we show activation maps illustrating how two highly important features, one in the middle transformer layer (layer -3) and one from the final layer (layer -1), activate over image patches. Both features appear to represent the same underlying concept: a flat surface such as floor or ground. This provides an example of a feature that remains constant across layers. One may think that the model has an excess of depth. However, for making a correct classification, some low-level features might need to coexist with other high-level features that do require additional processing across layers.

This example also reveals an interesting phenomenon: a last-layer feature that is important for task 1 but whose norm has faded at task 5 (Figure 7) re-emerges as an important task 5's feature in a middle layer. This might mirror the depth effects observed in section 4.1, where features learned earlier in the network fade as depth increases. Future continual learning methods could leverage this by restoring faded late-layer features that are also identified at earlier layers to mitigate forgetting.



Figure 13. Activation maps of layer -3's feature 167 learned in task 0, and layer -1's feature 131 learned in task 4. Shown are the images that most strongly activated this feature at each task.